
Stochastic Sparse Attention for Memory-Bound Inference

Kyle Lee¹ Corentin Delacour¹ Kevin Callahan-Coray¹ Kyle Jiang¹ Can Yaras² Samet Oymak²
Tathagata Srimani³ Kerem Y. Camsari¹

Abstract

Autoregressive decoding becomes bandwidth-limited at long contexts, as generating each token requires reading all n_k key and value vectors from KV cache. We present Stochastic Additive No-mulT Attention (SANTA), a method that sparsifies value-cache access by sampling $S \ll n_k$ indices from the post-softmax distribution and aggregates only those value rows. This yields an unbiased estimator of the post-softmax value aggregation while replacing value-stage multiply-accumulates with gather-and-add. We introduce stratified sampling to design variance-reduced, GPU-friendly variants, demonstrating $1.5\times$ decode-step attention kernel speedup over FlashInfer and FlashDecoding on an NVIDIA RTX 6000 Ada while matching baseline accuracy at 32k-token contexts. Finally, we propose Bernoulli qK^T sampling as a complementary technique to sparsify the score stage, reducing key-feature access through stochastic ternary queries. Both methods are orthogonal to upstream techniques such as ternary quantization, low-rank projections, and KV-cache compression. Together, they point toward sparse, multiplier-free, and energy-efficient inference. We open-source our kernels at: <https://github.com/OPUSLab/SANTA.git>

1. Introduction

Transformers (Vaswani et al., 2017) underpin modern language models (OpenAI, 2023; Touvron et al., 2023; Gemini Team et al., 2023). As deployments increasingly rely on long contexts, autoregressive decoding enters a regime where throughput is often limited by memory bandwidth:

¹Department of Electrical and Computer Engineering, University of California, Santa Barbara, CA, USA ²Department of Electrical and Computer Engineering, University of Michigan, Ann Arbor, MI, USA ³Department of Electrical and Computer Engineering, Carnegie Mellon University, Pittsburgh, PA, USA. Correspondence to: Kyle Lee <kylelee@ucsb.edu>.

generating each new token repeatedly streams the Key-Value (KV) cache for all prior tokens. For example, for Llama-3.1-8B-Instruct at a 32k-token context, streaming bf16 keys and values is on the order of ~ 128 MB *per layer per generated token*, and KV memory demands scale linearly with context length and batch size.

A broad literature mitigates this bottleneck from several angles. KV-cache quantization/compression reduces bytes per element (Liu et al., 2024; Hooper et al., 2024); cache-management policies reduce the number of retained tokens (Tang et al., 2024; Zhang et al., 2023); and structured sparsity or candidate selection reduces attention cost (Child et al., 2019; Zaheer et al., 2020; Beltagy et al., 2020; Wang et al., 2020; Kitaev et al., 2020; Chen et al., 2025). Architectural changes such as grouped-query attention (GQA) reduce KV footprint by sharing keys/values across heads (Ainslie et al., 2023), and decoding kernels improve IO locality for *exact* attention (Dao et al., 2023; Ye et al., 2025). However, even with optimized exact kernels, long-context decoding still incurs a persistent cost: each step touches essentially the full KV state.

We study a complementary inference-time lever: *reducing the amount of KV data accessed per decode step* without permanently discarding cache contents. Our primary focus is the post-softmax value aggregation, where dense attention computes AV by multiplying attention weights by all n_k value rows. We introduce **Stochastic Additive No-mulT Attention (SANTA)**, which samples $S \ll n_k$ indices from the post-softmax distribution and aggregates only those sampled rows of V via gather-and-add. This yields an *unbiased estimator of the post-softmax value aggregation* while reducing value-cache row reads per query from n_k to S (and eliminating value-stage multiplications in favor of additive accumulation). We further propose variance-reduced variants (**S²ANTA**) based on stratified and systematic sampling that bolster accuracy and admit GPU-friendly implementations. Since sparsifying V reads yields the clearest bandwidth benefit in decoding, our systems evaluation targets decode-step acceleration at long contexts.

On modern GPUs, these changes translate into measurable kernel-level gains: our S²ANTA CUDA kernels achieve up to $1.5\times$ **decode-step attention-kernel speedup** over

FlashInfer and FlashDecoding at 32k-token contexts while matching baseline accuracy on long-context prompts (Section 3).

Finally, we propose **Bernoulli qK^\top sampling** as a complementary technique for the score stage: it represents query elements as Bernoulli variables to form sparse ternary queries in $\{-1, 0, +1\}$, yielding an unbiased estimator of qK^\top and inducing feature-sparse key access during decoding. In this work, our implemented kernels and measured speedups are driven primarily by value-stage sparsification; Bernoulli qK^\top is presented as a complementary mechanism that can be combined with SANTA to sparsify both branches.

Contributions. Concretely, we: (i) introduce SANTA and variance-reduced S^2 ANTA as unbiased estimators of the post-softmax value aggregation that reduce value-cache reads from n_k to S ; (ii) design GPU kernels that parallelize sampling and sparse accumulation, demonstrating up to $1.5\times$ decode-step attention-kernel speedup over FlashInfer/FlashDecoding at 32k-token contexts while matching baseline accuracy; (iii) empirically characterize tunable accuracy–efficiency trade-offs on GSM8K, MMLU, and long-context benchmarks; and (iv) propose Bernoulli qK^\top sampling as a complementary score-stage estimator that can reduce key-feature access during decoding.

2. Stochastic Additive No-mult Attention (SANTA)

Stochastic Additive No-mult Attention (SANTA)

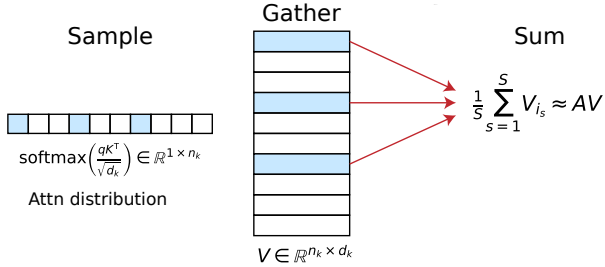


Figure 1. SANTA requires $S \ll n_k$ memory accesses to sampled rows of V , eliminating multiplications following the softmax operation. Normalization by S is a bit shift if S is a power of 2.

In principle, SANTA can be employed for the prefill or decode stages. Since the benefit of sparse memory access becomes apparent in decode, we present SANTA as a decoding algorithm. In autoregressive decoding, we consider a single query vector $q \in \mathbb{R}^{1 \times d_k}$. Scaled dot-product attention (SDPA) is expressed as a function of the key matrix and value matrix:

$$\text{Attn}(q, K, V) = \text{softmax}\left(\frac{qK^\top}{\sqrt{d_k}}\right) V = AV, \quad (1)$$

where $K \in \mathbb{R}^{n_k \times d_k}$ is the key matrix, $V \in \mathbb{R}^{n_k \times d_k}$ is the

value matrix, and $A \in \mathbb{R}^{1 \times n_k}$ represents the attention scores as a probability distribution.

To approximate AV , we treat A as a categorical distribution over keys and sample S indices i.i.d. from it (with replacement). For query vector q , we fetch the corresponding S rows of V and average them. This yields an estimate of the attention output using only row indexing and addition.

As an illustrative example, consider number of keys $n_k = 3$. We sample $S = 3$ one-hot attention vectors from the categorical distribution A :

$$\widehat{AV} = \frac{1}{3} ([1 \ 0 \ 0] + [1 \ 0 \ 0] + [0 \ 0 \ 1]) V, \quad (2)$$

which simplifies by distributivity of matrix multiplication over addition:

$$\begin{aligned} \widehat{AV} &= \frac{1}{3} ([1 \ 0 \ 0] V + [1 \ 0 \ 0] V + [0 \ 0 \ 1] V) \\ &= \frac{1}{3} (V_1 + V_1 + V_3). \end{aligned} \quad (3)$$

where each $V_i \in \mathbb{R}^{1 \times d_k}$ is a sampled row of V . The one-hot attention vectors in Eqs. 2, 3 are only for illustrative purposes; they represent an indexing and gather operation, and are not materialized as vectors in memory.

Finally, SANTA can be summarized as:

$$\widehat{AV} = \frac{1}{S} \sum_{s=1}^S V_{i_s} \approx AV, \quad (4)$$

where i_s is a sampled index and each V_{i_s} denotes a gathered row from V . Multiplications in the value stage have therefore been eliminated in favor of sampling, indexing and addition. If S is chosen as a power of 2 (and the model has a fixed point representation), normalization may be implemented as a bit-shift. Fig. 1 illustrates SANTA’s memory access benefits for autoregressive decoding: SANTA sparsely reads only $S \ll n_k$ sampled rows of V and computes an additive average without multiplications after the softmax.

We provide a formal mathematical description of SANTA in Appendix A. SANTA is an unbiased estimator of the attention function whose variance scales as $1/S$ (Appendix A.1, A.2). A dimension-free high-probability concentration bound for SANTA is deferred to Appendix B.

2.1. S^2 ANTA: stratified and systematic sampling

S^2 ANTA reduces variance via stratified sampling: dividing the CDF into S equal probability mass intervals and sampling once per interval for better coverage of the attention distribution. We devise two variants: independent stratified sampling (S^2 ANTA-strat) and systematic sampling (S^2 ANTA-sys).

The mechanics of S^2 ANTA-strat remain identical to default SANTA, except the S samples are drawn per stratum instead of iid from the full distribution. Systematic sampling (S^2 ANTA-sys) similarly splits the attention distribution CDF into S equal probability mass partitions. However, whereas independent stratified sampling draws S random offsets for each of S strata, systematic sampling draws a single offset U and applies the same offset to all strata, effectively drawing S samples with a single random number.

Construction. Fix a query q . Let $A_q = (p_{q1}, \dots, p_{qn_k})$ be the attention weights and F_q the associated CDF on $[0, 1)$. Partition $[0, 1)$ into S equal intervals

$$I_m := [m/S, (m+1)/S), \quad m = 0, \dots, S-1.$$

Define two schemes:

- **Independent stratified (S^2 ANTA-strat).** Draw $T_m \sim \text{Unif}(I_m)$ independently for $m = 0, \dots, S-1$, set $J_m := F_q^{-1}(T_m)$, and output $\widehat{AV}_q^{\text{ind}} := \frac{1}{S} \sum_{m=0}^{S-1} V_{J_m}$.
- **Systematic (S^2 ANTA-sys).** Draw a single $U \sim \text{Unif}([0, 1/S))$ and take thresholds $T_m := U + m/S$. With $J_m := F_q^{-1}(T_m)$, output $\widehat{AV}_q^{\text{sys}} := \frac{1}{S} \sum_{m=0}^{S-1} V_{J_m}$.

S^2 ANTA-strat and S^2 ANTA-sys are unbiased estimators of attention (see Appendix A.4). Only S^2 ANTA-strat has a theoretical guarantee of variance reduction compared to default SANTA (see Appendix A.5). Despite lacking a variance reduction guarantee, we validate that S^2 ANTA-sys exhibits comparable performance to S^2 ANTA-strat on reasoning benchmarks and long-context benchmarks. S^2 ANTA-sys demonstrates similar variance reduction to S^2 ANTA-strat in practice (see Appendix D). Systematic sampling with S^2 ANTA-sys is appealing because it draws samples using one random number instead of S random numbers, which may be easier to implement in hardware.

2.2. Theoretical operations and memory accesses

By virtue of SANTA’s sparsity, in autoregressive decoding, SANTA demonstrates a S/n_k reduction in post-softmax additions and reads to rows of V , where S is the sample budget and n_k is the number of keys. SANTA removes post-softmax multiplications in favor of additive accumulation (see Appendix E for analysis of decode-step operations and memory accesses).

In prefill, while similar arguments hold for SANTA’s reduced additions and removed multiplies, there is no longer sparse memory access to the value matrix V . Each of $n_q = n_k$ queries may each sample S rows of V , therefore

requiring $\gg S$ rows of V when the union across all queries is considered (see Appendices F, G for prefill analysis).

3. GPU kernels for variance-reduced SANTA

Section 2 introduced SANTA and variance-reduced sampling rules (stratified/systematic), which specify *what* to sample to form an unbiased estimator of the value-stage aggregation AV . In this section we focus on *how* to realize these samplers efficiently at decode time on GPUs: we introduce two kernel strategies, S^2 ANTA-prop and S^2 ANTA-flash, which differ in how they allocate samples across tiles (global proportional allocation vs. speculative per-tile sampling with deferred normalization).

3.1. Parallelizing stochastic attention on GPUs

Efficient implementation on GPUs presents a unique systems challenge: parallelizing the sampling control flow. Standard attention (SDPA) is amenable to “split-KV” strategies (e.g., FlashDecoding (Dao et al., 2023)) because the reduction of values is associative: partial sums can be computed locally and merged later. Sampling, however, creates a sequential dependency: determining *which* rows of V to access generally requires a global Cumulative Distribution Function (CDF). A naive implementation would require a sequential pass over the global probability distribution to draw sample indices, leaving the GPU compute units idle and preventing parallel access to the value matrix.

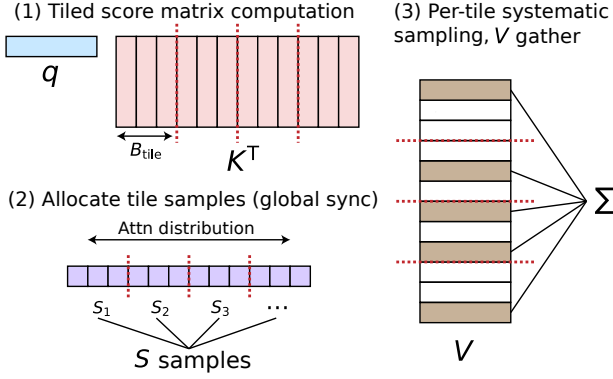
To unlock parallel V -access, we must determine the number of samples per tile *before* or *independently* of the full global reduction. We propose two strategies to break this dependency:

1. **Proportional Sample Allocation (S^2 ANTA-prop):** We pre-calculate the probability mass of each tile to deterministically assign sample budgets. This requires a global barrier but ensures exact load balancing.
2. **Speculative Local Sampling (S^2 ANTA-flash):** Tiles sample independently with uniform budgets, speculating that all tiles are equally important, followed by a post-hoc re-weighting. This removes the barrier but introduces sample waste.

We implement both strategies and evaluate their decode-step kernel latency and long-context accuracy at 32k-token prompts in Section 3.4.

3.2. S^2 ANTA-prop: exact budget allocation via global sync

S^2 ANTA-prop (Figure 2) breaks the sequential sampling dependency by resolving the global partition function Z in a lightweight initial pass.

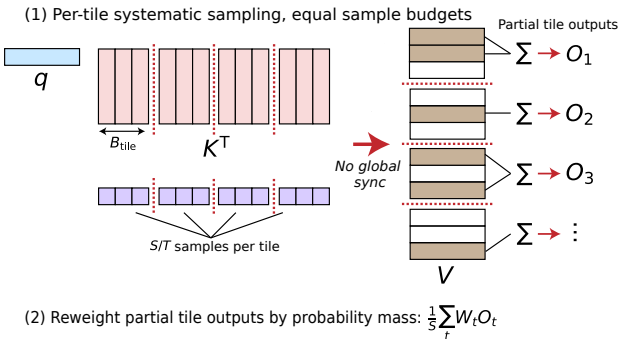

 Figure 2. S^2 ANTA-prop kernel overview.

The algorithm proceeds in three stages. The key dimension n_k is partitioned into tiles of length B_{tile} .

- Pass 1 (score stash & tile stats):** We compute attention scores exactly. The exponentiated scores (or a normalized equivalent) are written to global memory. Crucially, since the scores are scalars ($1 \times n_k$) while the values are vectors ($n_k \times d_k$), this stash consumes negligible bandwidth ($1/d_k$) compared to a full value fetch. We also compute and write local partition functions Z_{tile} .
- Global budget allocation:** A separate kernel sums the tile statistics to find the global Z . It then assigns a specific sample count to each tile: $S_{\text{tile}} \propto S \cdot (Z_{\text{tile}}/Z)$.
- Pass 2 (parallel gather):** Using the stashed scores and the assigned S_{tile} , each tile systematically samples indices and accumulates rows from V . Tiles with low probability mass are assigned $S_{\text{tile}} = 0$, allowing them to skip the expensive V -read entirely.

Comprehensive pseudocode is in Appendix O.

3.3. S^2 ANTA-flash: Speculative Sampling with Deferred Normalization


 Figure 3. S^2 ANTA-flash kernel overview.

To eliminate the latency of the global synchronization barrier, S^2 ANTA-flash (Figure 3) adopts a speculative approach structurally similar to FlashDecoding.

Instead of pre-calculating the global budget, each tile is allocated a fixed, uniform budget $S_{\text{tile}} \approx S/T$, where T is the number of tiles. Each tile samples locally *as if* it contained the entire probability mass. A second reduction kernel then computes the true global partition function Z and down-weights the partial outputs of tiles that had low probability mass.

This method maximizes parallelism by removing the global barrier but suffers from *sample waste*: tiles with low probability mass still consume compute and bandwidth to draw samples that are effectively down-weighted during the final merge. In our 32k-token evaluation (Section 3.4), matching SDPA accuracy requires substantially larger budgets for S^2 ANTA-flash; the accuracy-matching operating point is $S=2048$ for S^2 ANTA-flash versus $S=128$ for S^2 ANTA-prop (Table 1). See Appendix P for full pseudocode.

3.4. Kernel results at long contexts (32k)

We evaluate decode-step attention *kernel latency* together with end-task *accuracy* in the long-context decoding regime. Within this section, SDPA is used for prefill and only the *decode step* uses S^2 ANTA. Kernel timings are reported for a single decoding step on an NVIDIA RTX 6000 Ada GPU (batch size 1) using Llama-3.1-8B-Instruct (Meta AI, 2024) tensor shapes; we compare against optimized FlashInfer and FlashDecoding backends. The measurement protocol and tensor layouts are provided in Appendix Q.

To make latency comparisons meaningful, we select one operating point per kernel family as the *smallest* sample budget S that matches SDPA accuracy on 32k-token long-context tasks. This yields $S=128$ for S^2 ANTA-prop and $S=2048$ for S^2 ANTA-flash. These are exactly the configurations that deliver $\approx 1.5\times$ decode-step attention-kernel speedup in Fig. 4 while matching SDPA within confidence intervals in Table 1.

We next verify that these speedup points preserve long-context accuracy. We evaluate on tasks from RULER (Hsieh et al., 2024) using 32,768-token prompts: frequent-word extraction (FWE), needle-in-a-haystack (NIAH), single-hop QA (QA₁, derived from SQuAD (Rajpurkar et al., 2018)), and multi-hop QA (QA₂, derived from HotpotQA (Yang et al., 2018)). Results are shown in Table 1.

At these operating points, the speedups are driven primarily by reduced memory traffic from sparsifying reads of the value matrix V . For S^2 ANTA-prop, $S=128$ corresponds to extremely sparse value access at 32k contexts (e.g., $\lesssim 1.56\%$ V access when accounting for GQA). S^2 ANTA-flash attains comparable speedup, but requires a larger total

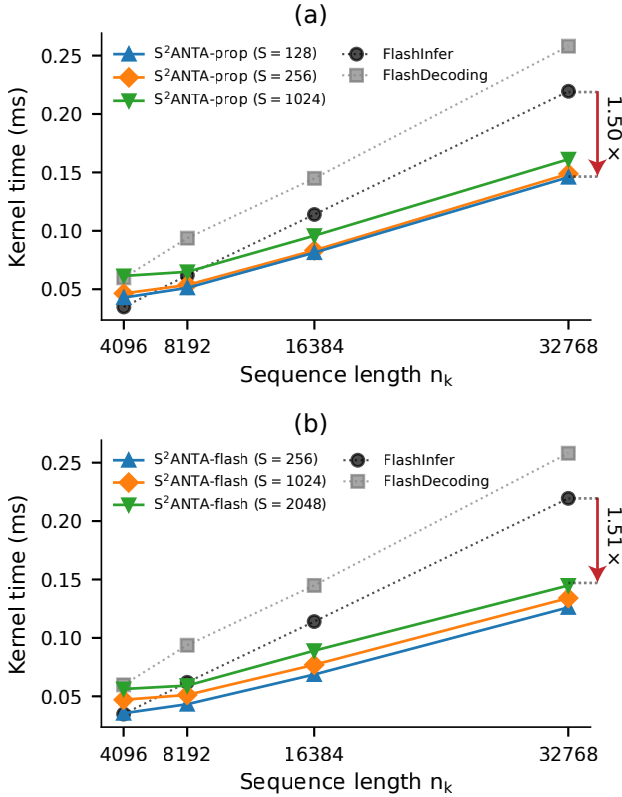


Figure 4. S^2 ANTA kernel latency on Llama 8B tensor shapes for 1 decoding step. (a) S^2 ANTA-prop demonstrates a $1.50\times$ speedup relative to FlashInfer at a 32k-token context. (b) S^2 ANTA-flash similarly exhibits a $1.51\times$ speedup. Both operating points ($S = 128$ for prop, $S = 2048$ for flash) correspond to configurations that recover baseline accuracy (Table 1).

sample budget because uniform per-tile sampling expends samples on low-mass tiles before the deferred renormalization step (“sample waste”).

These timings are kernel-level improvements; realized end-to-end speedups are subject to Amdahl’s Law and are largest in the memory-bound long-context regime (e.g., $n_k \gtrsim 8k$) where KV-cache streaming dominates decode time. While S^2 ANTA is multiplier-free in principle, current GPUs are highly optimized for dense fused multiply-accumulate instructions; we therefore view multiplier-free arithmetic as an additional energy-oriented benefit that may become more pronounced on future hardware.

Additional benchmark results for 8k-token contexts are available in Appendix R.

3.5. Energy considerations

Beyond latency, S^2 ANTA’s design offers two complementary paths to energy reduction. First, sparse memory access reduces value-cache traffic from n_k to S rows per query, at accuracy-matching operating points, this corresponds to

Table 1. Accuracy of Llama 8B on 4 long-context tasks with a 32,768-token prompt. SDPA is used in prefill. Tasks: frequent word extraction (FWE), needle-in-a-haystack (NIAH), single-hop QA (QA₁), multi-hop QA (QA₂). S : sample budget. Accuracy shows 95% bootstrap confidence intervals.

Kernel	S	FWE	NIAH	QA ₁	QA ₂
S^2 ANTA-prop	128	95.40±1.10	98.25±0.62	64.40±4.50	60.20±4.20
S^2 ANTA-prop	256	95.47±1.10	98.50±0.57	63.40±4.10	60.60±4.00
S^2 ANTA-prop	1024	95.40±1.07	98.40±0.60	64.20±4.00	59.60±4.40
S^2 ANTA-flash	256	66.20±2.40	88.95±1.43	63.00±4.20	57.20±4.30
S^2 ANTA-flash	1024	91.60±1.43	98.10±0.62	62.20±4.10	61.00±4.30
S^2 ANTA-flash	2048	94.13±1.13	98.25±0.62	64.60±4.20	60.00±4.40
SDPA (baseline)	—	95.60±1.00	98.35±0.62	64.00±4.10	58.80±4.10

$>90\%$ reductions in value-stage memory access at 32k contexts. Second, replacing dense multiply-accumulate with gather-and-add eliminates multiplication operations entirely. While our current GPU kernels primarily exploit the first benefit, hardware architectures optimized for sparse, adder-centric computation could realize both. These characteristics make S^2 ANTA a natural fit for emerging AI accelerators where memory bandwidth and multiplier energy are primary constraints.

4. General reasoning & accuracy verification

In this section, we consider SANTA, S^2 ANTA-strat (stratified sampling), and S^2 ANTA-sys (systematic sampling) as mathematical constructions (as in Section 2), validating the methods’ accuracy on GSM8K, MMLU, and long-context benchmarks using PyTorch reference implementations. While demonstrated GPU kernel speedups are for autoregressive decoding, evaluations in this section use SANTA in both prefill and decoding. Since SANTA in principle reduces additions and V memory access by S/n_k and removes post-softmax multiplies, future adder-centric hardware may enable gains in energy efficiency in the compute-heavy prefill phase; for instance, on modern CMOS, a FP16 multiply typically costs 1.1 pJ vs. 0.4 pJ for an add (Horowitz, 2014).

4.1. GSM8K

We consider Llama-3.1-8B-Instruct (“Llama 8B”) (Meta AI, 2024) on the GSM8K dataset as a mathematical reasoning benchmark (Cobbe et al., 2021; OpenAI, 2023). Table 2 provides both accuracy and the average number of tokens (prompt + answer). Because the compute and memory access costs of SANTA are contextualized relative to the sequence length n_k , these sequence lengths justify the regimes where $S \ll n_k$ and SANTA is, in principle, cheaper than SDPA in attention’s value stage.

Default SANTA exhibits respectable performance, but

Table 2. GSM8K accuracy and average context length (prompt + answer) for Llama-3.1-8B-Instruct. S : SANTA sample budget. Accuracy shows 95% bootstrap confidence intervals.

S	S^2 ANTA-sys		S^2 ANTA-strat		SANTA	
	Acc. (%)	Tok.	Acc. (%)	Tok.	Acc. (%)	Tok.
2	1.11±0.34	1071	1.01±0.32	1071	1.26±0.34	1075
4	1.67±0.40	569	1.54±0.38	611	1.57±0.37	825
8	2.10±0.45	340	1.74±0.40	325	1.44±0.38	207
16	44.63±1.58	349	39.12±1.50	352	5.51±0.72	350
32	68.59±1.42	339	67.00±1.48	343	38.26±1.43	348
64	76.42±1.34	341	74.43±1.31	343	63.63±1.49	346
128	77.33±1.34	342	75.64±1.33	341	70.23±1.42	341
256	77.56±1.34	343	78.17±1.28	343	75.61±1.42	342
SDPA (baseline)					78.06±1.33	344

variance-reduced S^2 ANTA variants demonstrate superior performance across every sample budget S . S^2 ANTA implementations approach the accuracy of full SDPA (within 1%) while S remains shorter than the sequence length n_k , translating to memory-access savings and FLOP energy savings. In deployment settings where LLM users do not require maximum model performance, the sample budget S can be tuned to save computation cost. For instance, S^2 ANTA-sys achieves 76.42% accuracy at $S = 64$, which is about 19% of the average sequence length of $n_k = 341$ tokens. For a modest accuracy trade-off compared to SDPA’s 78.06%, S^2 ANTA-sys in principle costs 19% of the additions, 19% of the V -matrix accesses, and *no multiplies*.

We provide additional DeepSeek-R1-Distill-Qwen-7B (DeepSeek-AI, 2025) (DeepSeek 7B) results and comparisons to sparse top-k attention in Appendix H.

4.2. MMLU

Table 3. MMLU accuracy and average context length (prompt + answer) for Llama-3.1-8B-Instruct. S : SANTA sample budget. Accuracy shows 95% bootstrap confidence intervals.

S	S^2 ANTA-sys		S^2 ANTA-strat		SANTA	
	Acc. (%)	Tok.	Acc. (%)	Tok.	Acc. (%)	Tok.
2	24.52±1.22	1141	24.28±1.21	1141	24.89±1.27	1144
4	24.49±1.18	774	24.65±1.26	807	25.13±1.20	961
8	24.47±1.23	292	25.63±1.23	286	25.06±1.23	284
16	34.14±1.39	353	32.46±1.32	350	26.24±1.26	313
32	45.48±1.45	403	43.78±1.50	398	33.81±1.34	354
64	48.70±1.39	418	49.25±1.48	415	41.11±1.40	397
128	50.60±1.37	421	49.92±1.47	421	47.46±1.45	412
256	51.12±1.46	421	50.90±1.49	422	49.75±1.51	417
SDPA (baseline)					49.86±1.47	424

We further evaluate SANTA on the MMLU benchmark (Hendrycks et al., 2021; Center for AI Safety, 2024), which tests factual recall and general reasoning. MMLU benchmarking observes similar trends as GSM8K, where SANTA virtually recovers baseline accuracy at $S = 256$,

which is significantly shorter than the average sequence length $n_k = 417$. S^2 ANTA variants outperform default SANTA across S budgets of 64–256, recovering baseline SDPA accuracy (within 1%) with multiplier-free arithmetic and sparse memory access to rows of V since $S \ll n_k$. Extended results with DeepSeek 7B and top-k comparisons are provided in Appendix H.

4.3. Long context benchmarks

Table 4. Accuracy of Llama 8B on 4 long-context tasks with an 8k-token prompt. Tasks: frequent word extraction (FWE), needle-in-a-haystack (NIAH), single-hop QA (QA₁), multi-hop QA (QA₂). S : SANTA sample budget. Accuracy shows 95% bootstrap confidence intervals.

Kernel	S	FWE	NIAH	QA ₁	QA ₂
S^2 ANTA-sys	64	96.27±0.97	94.05±1.07	71.80±3.90	67.20±4.20
S^2 ANTA-sys	128	97.80±0.70	94.15±1.02	68.20±4.10	66.80±4.00
S^2 ANTA-sys	256	97.87±0.70	95.00±0.95	71.20±3.90	69.40±4.10
S^2 ANTA-strat	64	95.93±0.94	94.35±1.15	71.40±4.00	65.40±4.20
S^2 ANTA-strat	128	97.73±0.80	94.30±1.10	70.80±4.20	67.40±4.20
S^2 ANTA-strat	256	98.33±0.60	94.55±1.05	71.20±4.00	67.00±4.20
SANTA	64	92.53±1.27	93.95±1.30	64.60±4.20	63.40±4.20
SANTA	128	94.53±1.13	91.45±1.38	67.80±4.10	63.40±4.30
SANTA	256	96.20±0.93	93.15±1.18	68.00±4.10	66.40±4.10
SDPA (baseline)	—	98.53±0.60	94.55±1.00	71.80±3.90	68.60±4.20

We benchmark SANTA on long-context tasks borrowed from RULER (Hsieh et al., 2024) with a prompt length of 8192 tokens. The theoretical benefit of S^2 ANTA’s sparse computation is most stark in this long-context regime. With a budget of $S = 256$ in an 8192-token sequence, S^2 ANTA uses just $S/n_k = 3.125\%$ of the value-stage additions and memory accesses compared to full attention (following Table 8). It achieves this while using **no multiplications** and recovering baseline SDPA accuracy (within $\pm 1\%$) across every task.

For full clarity, when Llama 8B’s grouped-query attention (Ainslie et al., 2023) with 4 grouped queries is fully accounted for, then memory access to unique rows of V can in the worst case reach 12.5%, which remains extremely sparse. Extended results with top-k comparisons are provided in Appendix H.

5. Bernoulli qK^T for sparse key access

SANTA reduces memory access for the value matrix by sampling from the softmax distribution; however, it leaves the score computation (qK^T) intact. As illustrated in Fig. 5, we demonstrate that Bernoulli sampling of the query naturally zeroes out query-irrelevant features, thereby effectively reducing memory access for the key matrix.

We propose representing each query element as an independent Bernoulli variable, allowing the corresponding key

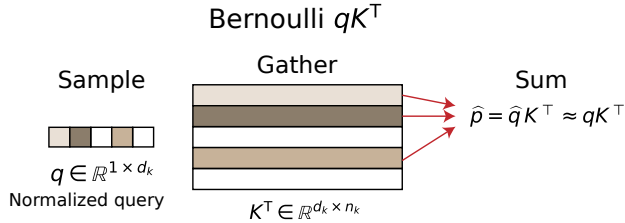


Figure 5. Bernoulli qK^T represents elements of the query vector as Bernoulli probabilities, sparsifying along the feature dimension d_k with multiplier-free arithmetic.

feature to be pruned when the sampling probability is low. While this method is applicable to the prefill phase, it induces sparse key access specifically during decoding; therefore, we focus on a single query q . First, the query vector is normalized as $q \leftarrow q/\text{norm}$, where $\text{norm} \geq \max_i |q_i|$. This ensures that each element $q_i \in [-1, 1]$ can be interpreted as a probability. Next, we estimate the product $p = qK^T$ as:

$$\hat{p} = \frac{\text{norm}}{B} \sum_{n=1}^B \hat{q}^{(n)} K^T, \quad (5)$$

where B is the sample count and $\hat{q}^{(n)}$ is a sparse ternary vector constructed via Bernoulli sampling (detailed in Appendix C). The linearity of expectation ensures this estimator is unbiased. Because $\hat{q}^{(n)}$ contains only values in $\{-1, 0, +1\}$, \hat{p} can be computed without multiplications by gathering and accumulating selected rows of K^T , followed by normalizing bit shifts for fixed-point representations.

Table 5 shows GSM8K results for Bernoulli qK^T applied to BitNet 2B (Ma et al., 2025) for both prefill and decoding. Using $B = 4$ stratified samples nearly recovers the accuracy of standard SDPA for the GSM8K benchmark, although the approximated scores typically have a 30% error (Appendix C.1). This suggests that the qK^T product within the highly quantized BitNet 2B architecture can tolerate numerical errors while maintaining strong overall performance.

Crucially, Bernoulli qK^T enables sparse access to cached keys, a benefit that is uniquely effective during decoding (the prefill phase requires nearly all features). This is shown in Table 5: with $B = 4$, the model needs only 67.5% of key features per head (vs. $\sim 100\%$ for prefill), while maintaining accuracy within 2% of the SDPA baseline.

5.1. Mean group query

While Bernoulli qK^T effectively prunes irrelevant features for individual heads, Grouped Query Attention (GQA) (Ainslie et al., 2023) complicates this by sharing keys and values across multiple heads (e.g., groups of 4 in BitNet). Consequently, the set of accessed features becomes the union of those required by all queries in the group, significantly increasing memory traffic. Table 5 illustrates this

Table 5. Performance of Bernoulli qK^T (stratified) on GSM8K (BitNet 2B) with the test set evaluated three times, and confidence intervals obtained by bootstrapping.

Method	B	Acc. (%) (95% CI)	Avg. Tok.	K^T Access (%)	
				Head	Group
SDPA	–	65.7 ± 1.5	306.1	100	100
Bernoulli qK^T	1	1.9 ± 0.43	1478.6	25.6	65.8
	2	48.7 ± 1.4	345.9	46.3	88.0
	4	64.5 ± 1.5	309.4	67.5	97.9
	8	65.1 ± 1.5	316.9	82.6	99.8
	16	65.8 ± 1.5	317.7	91.1	100
Mean Group Query	2	48.6 ± 1.5	318.6	57.9	57.9
	4	63.8 ± 1.5	311.4	84.7	84.7
Bernoulli qK^T	8	65.6 ± 1.6	311.4	97.1	97.1
	16	66.2 ± 1.5	310.2	99.7	99.7

effect: with $B = 4$ samples, K^T access jumps from 67.5% per head to 97.9% for the group. To preserve sparsity in this scenario, we propose using a representative query m for the entire group, defined as the mean of the queries’ absolute values. We then construct the estimator \hat{m} for the mean query m via Monte Carlo sampling (detailed in Appendix C.2), which stochastically prunes the low-amplitude mean features.

With $B = 4$ samples, \hat{m} contains approximately 15% of zero elements, which allows fetching only 85% of key features for the group (Table 5). The product $p = qK^T$ for each query is finally estimated as:

$$\hat{p} = (\hat{m} \odot \frac{q}{m}) K^T, \quad (6)$$

where \odot denotes element-wise multiplication. In this scenario, calculating \hat{p} requires normalization by m to compensate for the bias introduced by the mean group query. As shown in Table 5, the resulting estimator achieves similar accuracy to the single-query configuration while saving 15% of key memory accesses. We employ the mean group query estimator (Eq. 6) in all the following experiments.

5.2. Long context benchmarks

We evaluate our method on long-context tasks using Llama 8B, applying Bernoulli qK^T strictly during decoding since prefill requires full feature access. As detailed in Table 6, using $B = 8$ samples reduces key feature access to 72.8% for Llama 8B, with minimal accuracy loss ($< 2\%$ on NIAH, QA₁, and QA₂). Furthermore, this experiment highlights that key memory access patterns vary significantly across models. In contrast to Llama 8B, BitNet 2B requires accessing 97.1% of features for the same budget ($B = 8$, Table 5), a difference we attribute to distinct query distributions.

Table 6. Accuracy of Llama 8B on 4 long-context tasks with a 4,096-token prompt. Tasks: frequent word extraction (FWE), needle-in-a-haystack (NIAH), single-hop QA (QA₁), multi-hop QA (QA₂). B : Bernoulli qK^T (mean group query) sample budget. Accuracy shows 95% bootstrap confidence intervals.

Kernel (qK^T)	B	K^T Access (%)	FWE	NIAH	QA ₁	QA ₂
Bernoulli	4	47.3	70.4±2.0	87.2±1.9	72.0±3.8	66.2±4.1
Bernoulli	8	72.8	89.4±1.4	93.8±1.4	73.6±3.9	70.2±3.9
Bernoulli	16	92.1	92.7±1.2	94.5±1.2	74.8±3.5	71.6±4.2
SDPA	-	-	94.0±1.1	95.0±1.2	73.8±3.8	70.8±4.0

5.3. Combining Bernoulli qK^T and SANTA

Combining SANTA with Bernoulli qK^T enables sparse key-value accesses during decoding while replacing the majority of multiplications with additions. Table 7 shows the accuracy for the GSM8K benchmark using BitNet 2B and $B = 4$ Bernoulli samples for the qK^T computation, as the number of SANTA samples S is varied for the value stage. Using $B = 4$ for queries and $S = 64$ for attention weights almost recovers the SDPA baseline with less than 2% accuracy drop. Critically, this combined approach reduces key access by 15.3% and value access by 89.2%.

Table 7. Performance of Bernoulli qK^T (mean group query) + SANTA on GSM8K (BitNet 2B) with the test set evaluated three times (CI computed by bootstrapping).

Config	Acc. (%)	Avg.	(K,V) Access (%)
	(95% CI)	Tok.	Group
SDPA	65.7 ± 1.5	306.1	(100, 100)
$B = 4, S = 8$	55.0 ± 1.6	319.2	(84.7, 2.4)
$B = 4, S = 16$	60.7 ± 1.5	313.3	(84.7, 3.7)
$B = 4, S = 32$	62.3 ± 1.5	308.4	(84.7, 6.2)
$B = 4, S = 64$	63.8 ± 1.5	304.6	(84.7, 10.8)
$B = 4, S = 128$	64.1 ± 1.5	303.2	(84.7, 14.3)

6. Related work

Exact attention kernels and memory-bound decoding. FlashAttention-style kernels optimize IO locality and utilization for *exact* attention, including decoding-focused variants (Dao et al., 2023; Ye et al., 2025). However, exact decoding still streams essentially the full KV state each step at long contexts. Our approach is complementary: rather than further optimizing a full KV scan, we reduce the amount of KV data accessed at runtime by sparsifying value-cache reads (and, for Bernoulli qK^T , key-feature reads).

Reducing KV footprint and retention. KV quantization/compression reduces bytes per KV element (Liu et al., 2024; Hooper et al., 2024), and weight-only quantization targets model parameters (Frantar et al., 2023; Dettmers et al., 2023). GQA reduces KV size via head sharing (Ainslie et al., 2023). Cache-management methods bound KV growth by

evicting or pruning tokens (Tang et al., 2024; Zhang et al., 2023), introducing approximation by permanently discarding state. SANTA and Bernoulli qK^T are orthogonal to these approaches: they reduce the *number of elements accessed* over whatever cache is retained, and therefore can stack with compression, GQA, and eviction.

Approximating attention and sampling vs. truncation.

Structured sparsity and low-rank approximations reduce attention cost (often in prefill) (Child et al., 2019; Zaheer et al., 2020; Beltagy et al., 2020; Wang et al., 2020). In decoding, candidate selection and query-pruning methods reduce the cost of identifying relevant tokens or approximating qK^T (Kitaev et al., 2020; Chen et al., 2025; Ribar et al., 2024). This is where our two methods differ in scope: **SANTA operates in the value stage and is orthogonal to score-stage approximations**, while **Bernoulli qK^T is an alternative score-stage estimator** that induces feature-sparse key access via stochastic ternary queries. Sampling-based attention approximations have also been explored (Kim & Ko, 2022). A direct deterministic baseline is top- k attention (Gupta et al., 2021), which reduces value reads by truncation but is biased. In contrast, SANTA provides an unbiased estimator of the post-softmax value aggregation with controllable variance, and we emphasize variance reduction (stratified/systematic sampling) together with GPU kernels that realize measured speedups in the memory-bound decoding regime.

7. Conclusion

Long-context autoregressive decoding is frequently constrained by memory bandwidth due to repeated KV-cache access. We introduced SANTA, a stochastic method that avoids streaming the full value cache by sampling $S \ll n_k$ value rows from the post-softmax distribution and aggregating them with sparse gather-and-add. SANTA is unbiased for the post-softmax value aggregation, admits practical variance reduction via S^2 ANTA stratified/systematic sampling, and provides a tunable accuracy-latency knob in the sample budget S . On modern GPUs, our observed speedups primarily come from reducing value-cache bandwidth: our S^2 ANTA kernels achieve up to a $1.5\times$ decode-step attention-kernel speedup over FlashInfer/FlashDecoding at 32k-token contexts while retaining baseline performance at modest budgets.

We also proposed Bernoulli qK^T sampling as a complementary, forward-looking mechanism for the score stage that reduces *key-feature* access during decoding via stochastic ternary queries, which can be combined with SANTA to sparsify both branches of attention. Beyond reduced memory bandwidth, the predominantly additive structure of both estimators may also be attractive for future adder-centric hardware and/or prefill, which we leave to future work.

Impact Statement

This paper presents work whose goal is to advance the field of machine learning. There are many potential societal consequences of our work, none of which we feel must be specifically highlighted here.

A. Formal description of SANTA

For query q , the SANTA estimator can be written as

$$\widehat{AV}_q = \frac{1}{S} \sum_{s=1}^S V_{i_{q,s}}, \quad i_{q,s} \sim \text{Categorical}(A_q). \quad (7)$$

Definition A.1 (SANTA estimator). Let $Q \in \mathbb{R}^{n_q \times d_k}$, $K \in \mathbb{R}^{n_k \times d_k}$, $A = \text{softmax}(QK^\top / \sqrt{d_k}) \in \mathbb{R}^{n_q \times n_k}$, and $V \in \mathbb{R}^{n_k \times d_k}$. For each query index $r \in \{1, \dots, n_q\}$, sample $i_{r,1}, \dots, i_{r,S} \stackrel{\text{i.i.d.}}{\sim} \text{Categorical}(A_r)$ and define $\widehat{AV}_r = \frac{1}{S} \sum_{s=1}^S V_{i_{r,s}}$. Stacking all queries gives $\widehat{AV} \in \mathbb{R}^{n_q \times d_k}$.

A.1. Unbiasedness of SANTA

Proposition A.2 (Unbiasedness). $\mathbb{E}[\widehat{AV}] = AV$.

Proof of Proposition A.2. Fix any q . Since $\Pr(i_{q,s} = j) = A_{qj}$,

$$\mathbb{E}[\widehat{AV}_q] = \frac{1}{S} \sum_{s=1}^S \sum_{j=1}^{n_k} A_{qj} V_j = \sum_{j=1}^{n_k} A_{qj} V_j = (AV)_q.$$

Linearity of expectation completes the result. \square

A.2. Variance of SANTA

Proposition A.3 (Variance scaling of SANTA). *The covariance of the SANTA estimator scales as $1/S$.*

Throughout this subsection, fix a query index $q \in \{1, \dots, n_q\}$. Let $A_q \in \Delta^{n_k-1}$ denote the attention weights over keys, write $p_{qj} \triangleq A_{qj}$, and let $\mu_q \triangleq \sum_{j=1}^{n_k} p_{qj} V_j = (AV)_q$ be the exact attention output for that query. Default SANTA draws $i_{q,1}, \dots, i_{q,S} \stackrel{\text{i.i.d.}}{\sim} \text{Categorical}(A_q)$ and returns

$$\widehat{AV}_q = \frac{1}{S} \sum_{s=1}^S V_{i_{q,s}} \in \mathbb{R}^{d_k}.$$

Define centered summands $X_s \triangleq V_{i_{q,s}} - \mu_q$ and the (query-specific) covariance $\Sigma_q \triangleq \text{Cov}(V_i) = \sum_{j=1}^{n_k} p_{qj} (V_j - \mu_q)(V_j - \mu_q)^\top$.

We now aim to show that SANTA's covariance scales as $1/S$ (Proposition A.3):

$$\mathbb{E}[\widehat{AV}_q] = \mu_q, \quad \text{Cov}(\widehat{AV}_q) = \frac{1}{S} \Sigma_q.$$

Equivalently, $\mathbb{E}[\|\widehat{AV}_q - \mu_q\|_2^2] = \frac{1}{S} \text{tr}(\Sigma_q)$.

Proof. Unbiasedness was shown in Proposition A.2. For the variance, write $\widehat{AV}_q - \mu_q = \frac{1}{S} \sum_{s=1}^S X_s$ with $\mathbb{E}[X_s] = 0$ and $\text{Cov}(X_s) = \Sigma_q$. The X_s are i.i.d., hence $\text{Cov}\left(\frac{1}{S} \sum_{s=1}^S X_s\right) = \frac{1}{S^2} \sum_{s=1}^S \text{Cov}(X_s) = \frac{1}{S} \Sigma_q$. Taking the trace gives the mean-squared error identity. \square

A.3. S^2 ANTA estimator

Proposition A.4 (Unbiasedness of S^2 ANTA). *Let $\mu_q := \sum_j p_{qj} V_j = (AV)_q$. Then $\mathbb{E}[\widehat{AV}_q^{\text{ind}}] = \mathbb{E}[\widehat{AV}_q^{\text{sys}}] = \mu_q$.*

The proof is shown in Section A.4.

Remark A.5 (Systematic vs. independent). S^2 ANTA-strat is unbiased and admits a variance-dominance theorem, guaranteeing lower variance than that of i.i.d. sampling with default SANTA (Section A.5). S^2 ANTA-sys is also unbiased, but does not provide tractable variance guarantees; empirically it performs comparably.

A.4. Unbiasedness of S^2 ANTA

Proof of Proposition A.4. For S^2 ANTA-strat,

$$\begin{aligned} \mathbb{E}[\widehat{AV}_q^{\text{ind}}] &= \frac{1}{S} \sum_{m=0}^{S-1} \mathbb{E}\left[V_{F_q^{-1}(T_m)}\right] \\ &= \int_0^1 \left(\sum_j \mathbf{1}\{F_q(j-1) \leq t < F_q(j)\} V_j \right) dt \\ &= \sum_j p_{qj} V_j \\ &= \mu_q. \end{aligned}$$

For S^2 ANTA-sys, observe that *marginally* each T_m is uniform on I_m (though dependent across m). By linearity of expectation, the sum of expectations is unchanged by this dependence, so the same integral argument applies; see Cochran (1977, Ch. 8) and Owen (2013). \square

A.5. Variance reduction for S^2 ANTA-strat

Theorem A.6 (Variance reduction for S^2 ANTA-strat). *Let $\Sigma_q := \sum_j p_{qj} (V_j - \mu_q)(V_j - \mu_q)^\top$ and define within-stratum covariances*

$$\Sigma_q^{(m)} := \text{Cov}\left(V_{F_q^{-1}(T)} \mid T \sim \text{Unif}(I_m)\right).$$

Then

$$\text{Cov}(\widehat{AV}_q^{\text{ind}}) = \frac{1}{S^2} \sum_{m=0}^{S-1} \Sigma_q^{(m)} \leq_{\text{Loewner}} \frac{1}{S} \Sigma_q = \text{Cov}(\widehat{AV}_q),$$

with strict improvement unless all stratum means coincide. See Lohr (2010, Ch. 4) and Cochran (1977, Ch. 5).

Proof. Independence across strata gives $\text{Cov}(\widehat{AV}_q^{\text{ind}}) = \frac{1}{S^2} \sum_m \text{Cov}(V_{F_q^{-1}(T)} | T \in I_m)$. By the law of total covariance with $T \sim \text{Unif}(0, 1)$ and partition $\{I_m\}$,

$$\begin{aligned} \Sigma_q &= \mathbb{E} \left[\text{Cov}(V_{F_q^{-1}(T)} | T \in I_m) \right] \\ &\quad + \text{Cov} \left(\mathbb{E}[V_{F_q^{-1}(T)} | T \in I_m] \right) \\ &\geq_{\text{Loewner}} \mathbb{E} \left[\text{Cov}(V_{F_q^{-1}(T)} | T \in I_m) \right]. \end{aligned}$$

and averaging then dividing by S yields the claim. Strictness holds unless the stratum means are all equal. \square

Corollary A.7 (MSE ordering). *For any q ,* $\mathbb{E}[\|\widehat{AV}_q^{\text{ind}} - \mu_q\|_2^2] \leq \mathbb{E}[\|\widehat{AV}_q - \mu_q\|_2^2] = \frac{1}{S} \text{tr}(\Sigma_q)$.

B. Vector Bernstein tail for SANTA

Theorem B.1 (Vector Bernstein tail for SANTA). *Assume a uniform almost-sure bound $\|V_j - \mu_q\|_2 \leq V_{\max}$ for all j (hence $\|X_s\|_2 \leq V_{\max}$). Let $v_q \triangleq \mathbb{E}[\|V_i - \mu_q\|_2^2] = \text{tr}(\Sigma_q)$. Then for all $t > 0$,*

$$\Pr \left(\|\widehat{AV}_q - \mu_q\|_2 \geq t \right) \leq 2 \exp \left(- \frac{S t^2}{2(v_q + V_{\max} t/3)} \right).$$

Equivalently, with probability at least $1 - \delta$,

$$\|\widehat{AV}_q - \mu_q\|_2 \leq \sqrt{\frac{2v_q \log(2/\delta)}{S}} + \frac{2V_{\max} \log(2/\delta)}{3S}.$$

Proof sketch. This is a Hilbert-space (vector) Bernstein inequality: apply Bernstein to the mean of independent, mean-zero, L -bounded vectors with variance proxy v_q ; see, e.g., Boucheron et al. (2013, Thm. 2.10; see also Cor. 2.11) and Pinelis (1994). \square

C. Estimating qK^\top via Bernoulli sampling

We first normalize the query vector as $q \leftarrow q/\text{norm}$, where $\text{norm} \geq \max_i |q_i|$ so that each element $q_i \in [-1, 1]$ is interpreted as a probability. Then, we introduce the unbiased query estimator \widehat{q} where each element \widehat{q}_i is an independent ternary Bernoulli variable:

$$\begin{aligned} b_i &\sim \text{Bernoulli}(|q_i|), \\ \widehat{q}_i &= b_i \times \text{sign}(q_i) \in \{-1, 0, +1\}. \end{aligned} \quad (8)$$

Sampling from \widehat{q} provides an unbiased estimator for the product $p = qK^\top$:

$$\widehat{p} = \frac{\text{norm}}{B} \sum_{n=1}^B \widehat{q}^{(n)} K^\top, \quad (9)$$

where $\widehat{q}^{(n)}$ is a Bernoulli query vector, and B is the number of samples.

C.1. Bernoulli qK^\top error

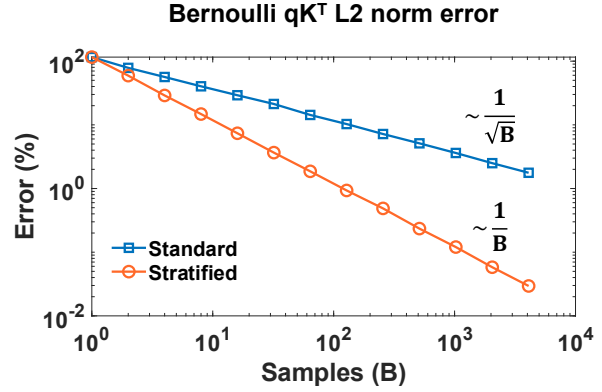


Figure 6. Mean L2 norm error for Bernoulli qK^\top . The score error is calculated during decoding with $d_k = 128$, a context length $n_k = 1024$, and averaged over 100 instances $q \sim \mathcal{N}(0, 1)$, $K \sim \mathcal{N}(0, 1)/\sqrt{d_k}$, $V \sim \mathcal{N}(0, 1)$.

Fig. 6 shows the scaling of the L2 norm error with the number of samples B , defined as $e = \|\widehat{p} - p\|_2 / \|p\|_2$. In similar fashion as SANTA, stratified Bernoulli sampling reduces the variance of each independent element \widehat{p}_i . The variance scales as $O(1/B^2)$, resulting in an overall L2 norm scaling as $O(1/B)$. For this numerical experiment, which uses a head dimension $d_k = 128$ and a context length $n_k = 1024$, using only $B = 4$ samples induces a mean L2 norm error of approximately 60% for standard Bernoulli sampling, compared to a much lower 30% for stratified sampling.

C.2. qK^\top for Grouped Query Attention

To maintain sparse key access when keys share multiple queries, as in GQA, we define a common representative query for the group, such as the mean of the absolute values of the queries:

$$m = \frac{1}{|\mathcal{G}|} \sum_{g \in \mathcal{G}} |q_g|, \quad (10)$$

where \mathcal{G} denotes the query group. We then estimate the mean query using Monte Carlo sampling, after normalizing by $\text{norm} \geq \max_i m_i$:

$$b_i \sim \text{Bernoulli}(m_i/\text{norm}) \quad (11)$$

$$\widehat{m} = \frac{\text{norm}}{B} \sum_{n=1}^B b^{(n)} \quad (12)$$

where $b^{(n)}$ are Bernoulli query vectors with independent elements b_i . After fetching the corresponding K^\top rows corresponding to non-zero elements of \widehat{m} , the product $p =$

qK^\top for each query is estimated as:

$$\hat{p} = \left(\hat{m} \odot \frac{q}{m}\right)K^\top, \quad (13)$$

where \odot denotes element-wise multiplication. In this mean group query scenario, calculating \hat{p} requires multiplications by the original query q and normalization by m to compensate for the bias introduced by the mean query approximation.

D. Empirical variance

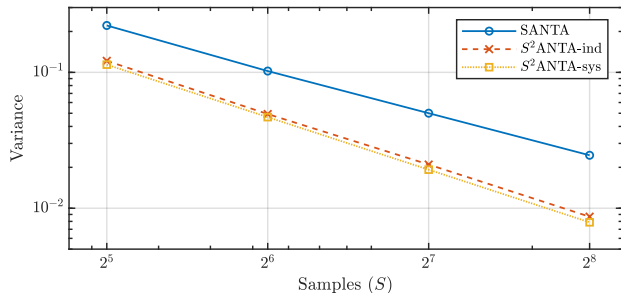


Figure 7. Empirical variance of SANTA on single-hop QA prompts (8k tokens).

To further validate our results, we empirically measure the variance of SANTA, S^2 ANTA-strat, and S^2 ANTA-sys. We sweep the sample budget S on 8k-token single-hop QA prompts, averaged across model layers and 30 prompts (normalized per head). S^2 ANTA variants exhibit significantly lower variance than SANTA. Though systematic sampling admits no tractable theoretical variance guarantees, it empirically demonstrates similar variance to independent stratified sampling (and requires 1 random number per query instead of S random numbers). On a log-log scale, slopes for SANTA, S^2 ANTA-strat, and S^2 ANTA-sys are -1.1 , -1.27 , and -1.29 , respectively, matching the $1/S$ scaling prescribed by theory (see Appendix M for details regarding the measurement protocol).

E. Theoretical operations and memory accesses in autoregressive decoding

Table 8. Per-query, per-head value-stage compute and memory for dense scaled dot-product attention (SDPA) and SANTA. n_k is the number of keys, d_k is the head dimension, and S is the SANTA sample budget per query. Value reads counts V elements accessed per query; Writes counts output elements.

Metric	SDPA	SANTA
Adds	$n_k d_k$	$S d_k$
Mults / Divs	$n_k d_k$	d_k
Value reads	$n_k d_k$	$S d_k$
Writes	d_k	d_k

Table 8 displays the theoretical additions, multiplications, and memory accesses incurred by SANTA in the value stage of attention, where the attention scores A multiply V . The score computation qK^\top is similar for both SANTA and SDPA, and is therefore omitted in this analysis (see Appendix G). We count individual scalar elements which are added together, multiplied together, or accessed by memory. Architecture-dependent effects such as multiply-accumulate (MAC) instructions, caching effects, or operation parallelism are not accounted for; arguments are fundamental and hardware-agnostic.

By virtue of SANTA’s sparsity, SANTA demonstrates a S/n_k reduction in post-softmax additions and reads to rows of V , where S is the sample budget and n_k is the number of keys (sequence length). A key distinction is that SANTA costs *fewer* additions than SDPA; SANTA does not seek to replace the multiplications in the AV computation, but rather, leverages sparse sampling to decrease the total number of additions while eliminating multiplications. So long as $S \ll n_k$, the advantage of attention sparsity holds true. Sampling overhead is not included; it is highly dependent on implementation, but drawing $S \ll n_k$ samples should be lightweight relative to memory accesses, multiplies, and adds (indeed, this proves to be the case with GPU kernel latency demonstrations in Section 3).

Whereas SDPA incurs $n_k d_k$ multiplications from computing dot products, SANTA only costs d_k normalizing multiplies by $1/S$. d_k is a constant model parameter and does not increase with the sequence length n_k . Furthermore, if S is chosen as a power of 2 and the model has a fixed point representation, this normalization may be implemented as a bit-shift.

In prefill, while similar arguments hold for SANTA’s reduced additions and multiplies, there is no longer sparse memory access to the value matrix V . Each of n_q queries may each sample S rows of V , therefore requiring $\gg S$ rows of V when the union across all queries is considered (see Appendices F, G).

F. Unique V -row coverage for SANTA prefill

Table 9. Unique V rows read (union over all query positions in a causal prefill pass), reported as a percentage of all n_k rows in the value matrix. Each entry is the mean over 10 trials and all attention heads, with Gaussian inputs $Q, K, V \sim \mathcal{N}(0, 1)$ (FP16), $H=32$ heads, and head dimension $d_k=128$.

S	Unique V rows read (% of n_k)				
	$n_k=1024$	2048	4096	8192	16384
1	49.90	50.04	49.96	49.95	49.95
4	79.95	80.00	79.96	79.96	79.95
8	88.92	88.83	88.86	88.86	88.85
16	94.07	94.11	94.10	94.09	94.08

Table 9 shows the percentage of unique V rows read by SANTA during prefill passes of differing sequence lengths n_k . Standard Gaussian distributed inputs Q, K, V are passed into SANTA with $d_k = 128$ and $H = 32$ heads for multi-headed attention. Even in the long-context, $S \ll n_k$ regime, any appreciable number of samples S results in SANTA sampling most rows of V when the union across all queries is considered. For $S = 16$, selected sequence lengths from $n_k = 1k - 16k$ show SANTA reading almost all ($> 94\%$) rows of V , because each of $n_q = n_k$ queries stochastically attend to S sampled keys. Therefore, while SANTA features sparse V access during autoregressive decoding, SANTA does *not* have apparent benefit from sparse memory access in prefill. Arguments concerning SANTA’s reduced addition and multiplication operations are still valid in prefill (Table 10).

G. Theoretical operations and memory accesses in prefill

Table 10. Per-head FLOPs and memory for scaled dot-product attention (SDPA), top- k , and SANTA. n_q : number of queries, n_k : number of keys, d_k : head dimension, k : top- k budget, S : SANTA sample budget per query. “Reads” count logical value/key elements accessed; “Writes” count output or score elements. Softmax, top- k selection, and sampling overheads are omitted.

Stage / Variant	Adds	Mults / Divs	Reads	Writes
Score stage (QK^T)				
SDPA / top- k / SANTA	$n_q n_k d_k$	$n_q n_k d_k$	$(n_q + n_k) d_k$	$n_q n_k$
Value stage				
SDPA	$n_q n_k d_k$	$n_q n_k d_k$	$n_q n_k d_k$	$n_q d_k$
Top- k	$n_q k d_k$	$n_q k d_k$	$n_q k d_k$	$n_q d_k$
SANTA	$n_q S d_k$	$n_q d_k$	$n_q S d_k$	$n_q d_k$

While SANTA’s apparent memory sparsity benefits are most viable in autoregressive decoding, for full clarity, this section provides generalized analysis for prefill. We consider the computational cost of SANTA, SDPA, and top- k attention, focusing on FLOPs and memory traffic in the value stage. Table 10 summarizes the theoretical costs per attention head. For the score stage (QK^T), the “Reads” entry $(n_q + n_k) d_k$ counts each query and key vector once per head, assuming they are loaded once from DRAM and then reused in on-chip memory during the matmul. In contrast, for the value stage we report $n_q n_k d_k$, $n_q k d_k$, and $n_q S d_k$ for dense SDPA, top- k , and SANTA, respectively, which count the per-query accesses rather than unique loads of elements from memory.

While top- k attention is memory-efficient and generally performs well, it introduces bias and can degrade significantly when the attention distribution is heavy-tailed. For example, recent work (Chen et al., 2025) shows that tasks such as common word extraction suffer when relevant information is not concentrated in the top- k entries. In contrast, stochas-

tic estimators like SANTA provide an unbiased estimate of full attention and retain robustness in such cases.

For both top- k and SANTA, we define a notion of compute budget, where k is the number of keys selected by top- k for each query of each attention head, while S is a sample budget representing the number of samples that SANTA draws for each query of each attention head. By default, we employ uniform S across model layers, though ablations suggest that S can be optimized per layer (Appendix I, J).

We omit softmax computation, top- k sorting overhead, and sampling from this analysis, as they are lightweight relative to memory accesses and the V matrix multiply, and are highly implementation-dependent. For example, many implementations use partial sorting (Samaga B L et al., 2024; Xie et al., 2025).

In both FLOPs and memory reads, SDPA scales as $n_q n_k$, reflecting the cost of full quadratic attention computation. Both top- k and SANTA reduce this to $n_q k$ and $n_q S$, respectively, assuming fixed budgets with $k, S \ll n_k$. This shifts the overall complexity of the value stage from quadratic to linear in sequence length, given a fixed budget k or S .

Top- k still incurs multiplication costs while SANTA eliminates multiplies. Top- k performs $n_q k d_k$ multiplications (per head), while SANTA requires only $n_q d_k$ divisions for normalization (if S is chosen as a power of 2, even these few divisions become simple bit-shifts).

H. Additional DeepSeek and top- k results

Table 11. GSM8K accuracy and average context length (prompt + answer) for DeepSeek-R1-Distill-Qwen-7B. k : number of keys in top- k , S : SANTA sample budget. Accuracy shows 95% bootstrap confidence intervals.

$k S$	Top- k		SANTA	
	Acc. (%)	Tok.	Acc. (%)	Tok.
2	0.23±0.15	4049	0.00±0.00	4217
4	23.88±1.31	3298	0.08±0.09	4208
8	72.25±1.35	2332	52.46±1.57	2799
16	82.51±1.21	1860	79.00±1.28	1778
32	86.23±1.02	1694	83.19±1.23	1667
64	86.76±1.03	1624	84.99±1.09	1587
128	87.54±1.02	1626	85.42±1.00	1594
256	88.20±0.97	1600	86.93±1.01	1627
SDPA (baseline)			88.75±1.00	1532

Tables 11, 12, 13, and 14 feature additional GSM8K and MMLU results with comparisons using DeepSeek-R1-Distill-Qwen-7B and top- k attention. Table 15 exhibits long-context benchmark results identical to Table 4, except with additional top- k comparisons.

Comparing SANTA and top- k requires care, as they have different computational profiles. We present results for sample

Table 12. GSM8K accuracy and average context length (prompt + answer) for Llama-3.1-8B-Instruct.

$k S$	Top- k		SANTA		S^2 ANTA-strat		S^2 ANTA-sys		
	Acc. (%)	Tok.	Acc. (%)	Tok.	Acc. (%)	Tok.	Acc. (%)	Tok.	
2	1.21±0.32	430	1.26±0.34	1075	1.01±0.32	1071	1.11±0.34	1071	
4	6.27±0.72	583	1.57±0.37	825	1.54±0.38	611	1.67±0.40	569	
8	41.32±1.50	549	1.44±0.38	207	1.74±0.40	325	2.10±0.45	340	
16	62.88±1.57	430	5.51±0.72	350	39.12±1.50	352	44.63±1.58	349	
32	72.50±1.34	384	38.26±1.43	348	67.00±1.48	343	68.59±1.42	339	
64	76.12±1.32	358	63.63±1.49	346	74.43±1.31	343	76.42±1.34	341	
128	77.13±1.30	349	70.23±1.42	341	75.64±1.33	341	77.33±1.34	342	
256	78.19±1.33	340	75.61±1.42	342	78.17±1.28	343	77.56±1.34	343	
SDPA (baseline)								78.06±1.33	344

Table 13. MMLU accuracy and average context length (prompt + answer) for DeepSeek-R1-Distill-Qwen-7B. k : number of keys in top- k , S : SANTA sample budget. Accuracy shows 95% bootstrap confidence intervals.

$k S$	Top- k		SANTA		
	Acc. (%)	Tok.	Acc. (%)	Tok.	
2	24.97±1.24	3598	4.33±0.58	4178	
4	38.93±1.32	2236	23.10±1.20	3666	
8	55.08±1.47	1659	44.55±1.47	2080	
16	59.07±1.36	1301	58.81±1.42	1506	
32	60.77±1.40	1173	61.05±1.45	1228	
64	62.03±1.38	1103	60.59±1.43	1104	
128	61.68±1.49	1061	62.38±1.32	1075	
256	62.05±1.46	1041	62.27±1.39	1074	
SDPA (baseline)				63.16±1.45	1020

budget S equal to the top- k budget k not as an iso-compute benchmark, but to demonstrate that SANTA achieves comparable or superior accuracy while using a fundamentally cheaper set of operations. At $S = k$: top- k costs $n_q k d_k$ multiplications + $n_q k d_k$ additions, whereas SANTA costs 0 multiplications + $n_q S d_k$ additions (Table 10).

A 32-bit FP multiply costs 3.7 pJ versus 0.9 pJ for addition (Horowitz, 2014). For equal budgets $k = S$, the value-stage energy consumption for the two methods are approximately: $k \times (3.7 + 0.9) = 4.6k$ pJ per element for top- k , vs. $S \times 0.9 = 0.9S$ pJ per element for SANTA. Relative to top- k , SANTA yields an $\approx 5\times$ energy reduction for value-stage FLOPs. We acknowledge that these are approximate energy estimates; we aim to provide hardware-agnostic comparisons, as modern GPU hardware is optimized for matmuls and contiguous memory access, while SANTA involves adds and sparse memory access.

Regarding memory accesses: SANTA’s accesses to elements of the V matrix scale as $n_q S d_k$, which in the worst case matches top- k ’s $n_q k d_k$ memory accesses at $k = S$. However, since SANTA samples with replacement, the number of unique keys is $\leq S$. In practice, as we quantify in Appendix L, the number of unique keys sampled is $< S$, which may offer significant caching advantages.

Table 14. MMLU accuracy and average context length (prompt + answer) for Llama-3.1-8B-Instruct.

$k S$	Top- k		SANTA		S^2 ANTA-strat		S^2 ANTA-sys		
	Acc. (%)	Tok.	Acc. (%)	Tok.	Acc. (%)	Tok.	Acc. (%)	Tok.	
2	23.56±1.20	588	24.89±1.27	1144	24.28±1.21	1141	24.52±1.22	1141	
4	28.37±1.27	359	25.13±1.20	961	24.65±1.26	807	24.49±1.18	774	
8	39.54±1.43	532	25.06±1.23	284	25.63±1.23	286	24.47±1.23	292	
16	45.26±1.37	484	26.24±1.26	313	32.46±1.32	350	34.14±1.39	353	
32	49.49±1.44	448	33.81±1.34	354	43.78±1.50	398	45.48±1.45	403	
64	48.33±1.37	433	41.11±1.40	397	49.25±1.48	415	48.70±1.39	418	
128	49.47±1.44	418	47.46±1.45	412	49.92±1.47	421	50.60±1.37	421	
256	49.75±1.43	421	49.75±1.51	417	50.90±1.49	422	51.12±1.46	421	
SDPA (baseline)								49.86±1.47	424

Table 15. Accuracy of Llama 8B on 4 long context tasks with an 8k-token prompt. Tasks: frequent word extraction (FWE), needle-in-a-haystack (NIAH), single-hop QA (QA₁), multi-hop QA (QA₂). k : number of keys for top- k . S : SANTA sample budget. Accuracy shows 95% bootstrap CIs.

Kernel	$k S$	FWE	NIAH	QA ₁	QA ₂
S^2 ANTA-sys	64	96.27±0.97	94.05±1.07	71.80±3.90	67.20±4.20
S^2 ANTA-sys	128	97.80±0.70	94.15±1.02	68.20±4.10	66.80±4.00
S^2 ANTA-sys	256	97.87±0.70	95.00±0.95	71.20±3.90	69.40±4.10
S^2 ANTA-strat	64	95.93±0.94	94.35±1.15	71.40±4.00	65.40±4.20
S^2 ANTA-strat	128	97.73±0.80	94.30±1.10	70.80±4.20	67.40±4.20
S^2 ANTA-strat	256	98.33±0.60	94.55±1.05	71.20±4.00	67.00±4.20
SANTA	64	92.53±1.27	93.95±1.30	64.60±4.20	63.40±4.20
SANTA	128	94.53±1.13	91.45±1.38	67.80±4.10	63.40±4.30
SANTA	256	96.20±0.93	93.15±1.18	68.00±4.10	66.40±4.10
SDPA (baseline)	—	98.53±0.60	94.55±1.00	71.80±3.90	68.60±4.20
top- k	64	93.07±1.20	92.55±1.10	65.60±4.10	60.80±4.10
top- k	128	95.40±0.96	93.60±1.15	69.20±3.90	62.20±4.50
top-k	256	97.27±0.80	94.55±1.05	70.60±3.90	64.20±4.10

For benchmarking, we apply SANTA and top- k to both pre-fill and autoregressive decoding. However, in practice, these sparse attention implementations may see greater benefit during decoding, when only a single query sparsely selects rows of V .

SANTA variants demonstrate strong performance relative to top- k on GSM8K and MMLU benchmarks, despite SANTA requiring no multiplications and a similar number of additions and memory accesses for $k = S$. However, the most remarkable result is shown in Table 15, where S^2 ANTA variants outperform top- k across virtually every long-context task for all $k = S$. S^2 ANTA’s lead over top- k is most apparent for multi-hop question answering (QA₂), where S^2 ANTA variants lead in performance by $\approx 5\%$ in several cases. It is plausible that long context tasks — multi-hop QA in particular — have information that is not concentrated in the top- k keys, and therefore SANTA’s unbiased estimate of attention outperforms top- k , which drops information and cannot attend to keys outside of the k largest attention scores.

I. Ablation study: one-hot attention samples

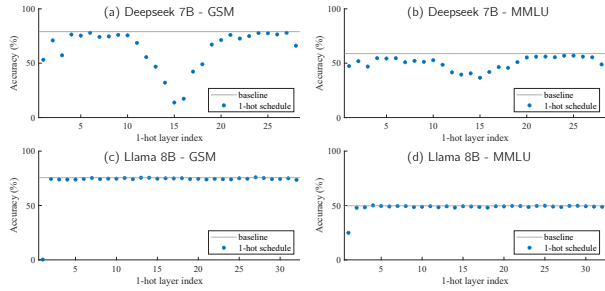


Figure 8. Ablations with one-hot stochastic attention. Baseline scores employ a fixed sampling budget of 16 and 256 for DeepSeek 7B and Llama 8B models, respectively. The horizontal axis shows the index of the model layer which is reduced to stochastic hard attention.

This section probes a fundamental question: how much does each attention layer matter? We find that one-hot stochastic attention, a limiting case of SANTA with $S = 1$, acts as a surprisingly sharp diagnostic. It reveals which transformer layers are robust to severe approximation and which are not, offering a practical lens into where attention precision matters most.

We perform these ablations by setting $S = 1$ in a single layer while keeping all other layers at fixed sample budgets: $S = 16$ for DeepSeek 7B (28 layers) and $S = 256$ for Llama 8B (32 layers). In this setting, each query attends to only one randomly sampled key, making that layer a hard attention bottleneck.

Models are evaluated on GSM8K and MMLU with the same protocol as Tables 2 and 3. The effect of this localized bottleneck on accuracy is summarized in Fig. 8. Some layers exhibit almost no degradation when ablated in this way, while others collapse entirely, most notably middle layers in DeepSeek 7B and the first layer in Llama 8B.

In DeepSeek 7B, layers 12–18 are highly sensitive to approximation, while early and final layers are much more tolerant. In contrast, Llama 8B exhibits extreme sensitivity in just the first layer. These patterns suggest that attention importance is neither uniform nor trivially architectural.

We observe similar qualitative trends regardless of the baseline sample budget; the $S = 16$ and $S = 256$ settings are arbitrary. The early-layer sensitivity in Llama 8B is consistent with prior findings on high-entropy attention in shallow layers (Clark et al., 2019), and with prior work that avoids approximating early layers (Tang et al., 2024; Sun et al., 2024). The middle-layer fragility in DeepSeek 7B remains an open and intriguing observation.

J. Layer-wise sample budget through RL

Algorithm 1 Layer-wise sample-budget optimization via REINFORCE

```

Require: initial logits  $\theta \in \mathbb{R}^{28}$  ( $\theta_i = 0$ ), total budget
 $N=224$ , learning-rate  $\alpha=0.02$ 
1: while training do
2:   Workers (in parallel):
3:   for  $e = 1, \dots, E$  do  $\{E=10$  episodes / worker run $\}$ 
4:     Compute  $p_i \leftarrow \exp(\theta_i) / \sum_j \exp(\theta_j)$ 
5:     Sample schedule  $\mathbf{S} \sim \text{Multinomial}(N, \mathbf{p})$ 
6:     Evaluate 16 GSM8K questions using schedule  $\mathbf{s}$ ;
       obtain reward  $r \in [0, 1]$ 
7:     Append  $(\mathbf{s}, r)$  to shared folder
8:   end for
9:
10:  Aggregator:
11:  Collect all new  $(\mathbf{s}^{(k)}, r^{(k)})$  tuples  $\{k = 1 \dots K\}$ 
12:  Compute baseline  $b \leftarrow \frac{1}{K} \sum_k r^{(k)}$ 
13:  Gradient:  $\mathbf{g} \leftarrow \frac{1}{K} \sum_k (r^{(k)} - b)(\mathbf{s}^{(k)} - N\mathbf{p})$ 
14:  Update logits  $\theta \leftarrow \theta + \alpha \mathbf{g}$ 
15:  Write back updated  $\theta$ 
16: end while

```

We now consider a global sample budget shared across all 28 transformer layers of DeepSeek 7B, allowing each layer to have a distinct sample count. We optimize this allocation using a REINFORCE-style algorithm (Williams, 1992), detailed in Algorithm 1.

We train the policy on the GSM8K training set. The policy logits $\theta \in \mathbb{R}^{28}$ define a softmax distribution over layers. At each iteration, we sample schedules using a multinomial draw over this distribution, with a total budget of 224 samples (i.e., 8×28). Each episode evaluates 16 questions; the reward is the fraction answered correctly. We intentionally starve the baseline with $S = 8$ samples per layer to create room for the learned schedule to improve.

Fig. 9 shows the final learned schedule after 501 iterations. The allocation aligns strikingly with the ablation trends from Fig. 8: more samples are assigned to the first and middle layers, where one-hot attention was most detrimental. That REINFORCE independently rediscovers this structure from only reward signals confirms that these patterns are not artifacts of the ablation method but instead are intrinsic to the models.

This experiment is not tuned for peak accuracy, but demonstrates that adaptive per-layer budgets meaningfully outperform fixed ones. Please see Appendix K for implementation details of distributed reinforcement learning using a Kubernetes compute cluster.

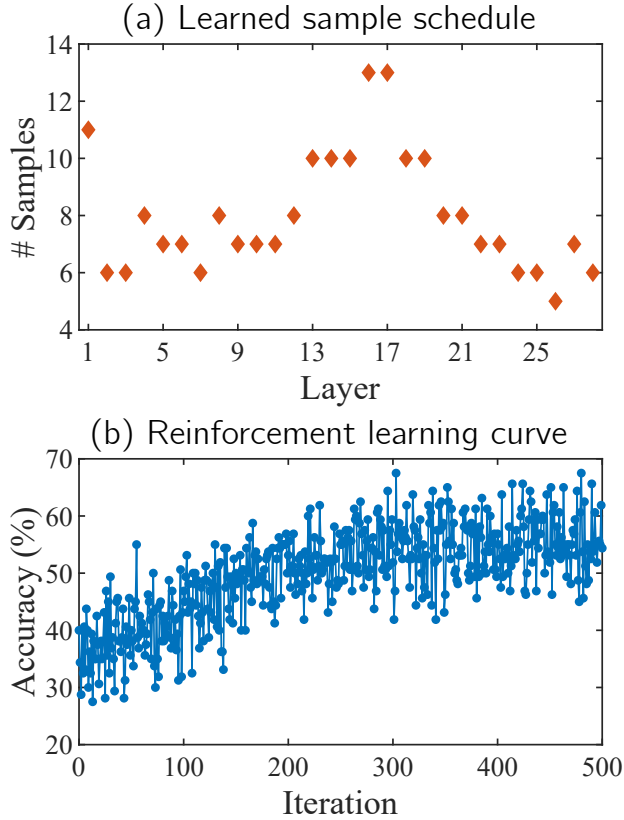


Figure 9. Learned schedule with a total budget of 224 samples across all 28 transformer blocks (DeepSeek 7B). (b) RL iterations over time.

Table 16. RL sample-schedule performance. Accuracy shows 95% bootstrap confidence intervals.

Schedule	Task	Accuracy (%)
Baseline (8 samples)	GSM8K	52.46 ± 1.47
Baseline (8 samples)	MMLU	44.55 ± 1.47
Learned schedule	GSM8K	66.06 ± 1.47
Learned schedule	MMLU	48.86 ± 1.53

K. Distributed reinforcement learning on Kubernetes

Topology. All pods mount a single read–write volume that serves as the rendezvous point.

- **Aggregator pod.** Holds the current policy and records a running history of baselines and gradients.
- **Worker pods.** Operate in a tight loop: (i) read the latest policy; (ii) sample a 28-dimensional schedule; (iii) evaluate ten batches of 16 questions; (iv) append a small JSON-lines result file to a designated “inbox” directory on the volume.

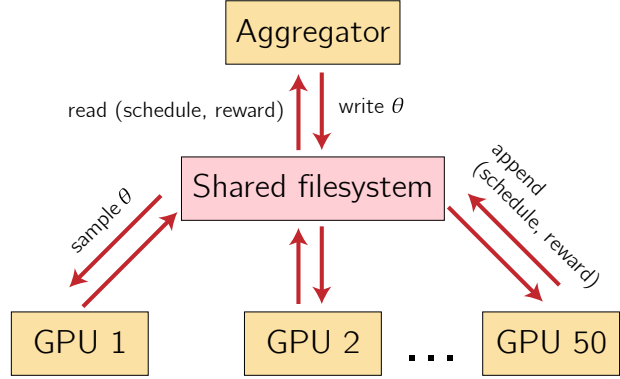


Figure 10. Kubernetes deployment schematic.

Aggregator loop. Whenever at least one new result file appears, the aggregator moves all current files into a private folder for the next iteration, computes the REINFORCE update and writes a new policy snapshot. It never pauses or signals the workers; it simply processes whatever has arrived. In practice, workers are unlikely to finish evaluation simultaneously, thus nearly every policy update comes from one worker output (10×16 questions). If two land together, the aggregator just uses a double-sized batch, which lowers the gradient’s variance.

Asynchrony and fault-tolerance.

- Workers can be terminated at any time; partial output vanishes harmlessly.
- Workers always proceed with the newest policy that has reached disk; no locking is needed.
- If the aggregator restarts it scans the history directory, resumes from the last completed iteration, and continues.

Scaling and resources. The worker Deployment’s replica count can be scaled up or down at any time during learning. For the 501 iterations in Fig. 9 we ran 50 GPU workers on a mix of RTX 3090, L4, and A10 cards (24 GB Ampere generation cards) for roughly 20 hours, totaling ≈ 1000 GPU-hours. The aggregator requests just one CPU core and a few hundred MiB of RAM.

Terminology. We keep the names aggregator and worker to highlight the simple “parameter-server” flavor of the design, but these roles align exactly with the common learner/actor split in distributed reinforcement learning.

L. Unique key-count

Since all versions of SANTA sample keys with replacement, the number of *unique* keys may be less than the sample budget S . In Table 17, we empirically measure the average

Table 17. Unique-key count vs. S (8192 tokens, single-query).

S	SANTA	S^2 ANTA-strat	S^2 ANTA-sys
32	11.0	12.7	13.0
64	16.7	21.2	21.7
128	25.9	35.8	36.4
256	38.3	60.3	61.6

number of unique keys sampled by the last query position for 8192-token single-hop QA prompts (normalized per head and averaged across model layers). This is indicative of the key diversity observed in autoregressive decoding. For a given S , S^2 ANTA variants achieve higher key diversity than default SANTA. Furthermore, the number of unique keys tends to be $\ll S$, implying that *fewer than* S unique rows of V require memory accesses. See Appendix M for details about the measurement protocol.

M. Implementation & measurement protocol for empirical variance and unique keys sampled

Setting. For a single layer/head at the last prefill position q^* , let the post-softmax attention over n_k keys be $p_j \geq 0$ with $\sum_{j=1}^{n_k} p_j = 1$, and let $V_j \in \mathbb{R}^{d_k}$ denote the corresponding value vectors. The dense-attention mean is

$$\mu = \sum_{j=1}^{n_k} p_j V_j \in \mathbb{R}^{d_k}.$$

SANTA estimator. Given a per-head sampling budget S , all SANTA variants estimate μ with

$$\widehat{AV} = \frac{1}{S} \sum_{s=1}^S V_{J_s},$$

where the key indices $\{J_s\}$ are drawn by one of three schemes: (i) multinomial; (ii) independent equal-mass stratified; or (iii) systematic (random-start, fixed-stride). These are the same variants used in the main paper; the code paths that implement them also record the per-head statistics described below at q^* .

M.1. What we measure (per head at q^*)

(1) Unique keys. The number of distinct keys touched by the sampler,

$$U := |\{J_1, \dots, J_S\}|,$$

upper-bounded by S (can be $< S$ if high-probability keys repeat). This is a proxy for how many memory locations each head actually reads.

(2) Variance trace of the estimator. We report the trace of the covariance (expected squared ℓ_2 error) of \widehat{AV} ,

$$\text{VarTrace}(\widehat{AV}) := \mathbb{E}[\|\widehat{AV} - \mu\|_2^2] = \text{tr}(\text{Cov}(\widehat{AV})),$$

specialized to each sampling scheme:

- **Multinomial (closed form).** Let $\Sigma := \sum_{j=1}^{n_k} p_j (V_j - \mu)(V_j - \mu)^\top$ so that $\text{tr}(\Sigma) = \sum_j p_j \|V_j\|_2^2 - \|\mu\|_2^2$. Then

$$\text{VarTrace}_{\text{multi}}(\widehat{AV}) = \frac{1}{S} \text{tr}(\Sigma).$$

- **Independent equal-mass stratified (closed form).** Partition $[0, 1]$ into S equal strata; for each stratum m , form the within-stratum discrete distribution induced by p and let Σ_m be the corresponding value covariance. Because draws across strata are independent,

$$\text{VarTrace}_{\text{strat}}(\widehat{AV}) = \frac{1}{S^2} \sum_{m=0}^{S-1} \text{tr}(\Sigma_m).$$

- **Systematic (replicate-based estimate).** There is no general closed form that holds uniformly for systematic sampling, so we estimate variance by repeated random starts. With $R \geq 2$ independent offsets, we compute $\widehat{AV}^{(r)}$ for each replicate, then use

$$\text{VarTrace}_{\text{sys}}(\widehat{AV}) = \frac{1}{R-1} \sum_{r=1}^R \|\widehat{AV}^{(r)} - \bar{V}\|_2^2,$$

$$\bar{V} = \frac{1}{R} \sum_{r=1}^R \widehat{AV}^{(r)}.$$

This estimator is applied per head at q^* .

M.2. How we aggregate and report

For each prompt, we compute U and the variance-trace scalar per head at q^* , then average over heads within a layer, average over layers, and finally average over prompts to obtain the quantities reported in the variance plots:

$$\bar{U}(S, \text{variant}) \quad \text{and} \quad \bar{T}(S, \text{variant}) = \overline{\text{VarTrace}}(\widehat{AV}).$$

This yields the curves summarized in the main text as a function of the budget S and the SANTA variant.

Protocol summary. All measurements use evaluation-mode forward passes, prefill-only, and record statistics *at the last token* per head; no additional dense attention pass is performed to form empirical errors. For multinomial and stratified we use the exact formulas above; for systematic we use the replicate-based estimator.

N. Prompting, Parsing, and Grading

In Section 4.1, we evaluate the GSM8K test split (1319 prompts) 3 times. Evaluation code uses straightforward answer parsing and borrows grading code from PRM800K (Lightman et al., 2024). For all runs, temperature = 0.6, top-p = 0.95, and repetition penalty = 1.1. We use left-padded batches of 8–16 prompts.

In Section 4.2, we average results over three runs on the MMLU validation set (1531 questions), using identical decoding parameters as GSM8K.

In Section 4.3, long-context benchmark results are averaged over 500 prompts and greedy decoding is employed with no repetition penalty applied.

DeepSeek 7B + GSM8K

Aspect	Procedure
Prompt	Question, blank line, then Please reason step by step, and put your final numeric answer within <code>\boxed{}</code> .
Answer extraction	Perform a brace-balanced search for the last occurrence of <code>\boxed{...}</code> (robust to nested braces). If none is found, fall back to the final ~200 characters of the model output.
Grading	Numeric equality judged by the MIT-licensed PRM800K grader; every prompt is counted, and blank or unparsable predictions score 0.

Table 18. Prompting and grading for DeepSeek 7B on GSM8K.

DeepSeek 7B + MMLU

Aspect	Procedure
Prompt	Question, four labeled choices, then Answer briefly. Put your final answer as a single letter inside <code>\boxed{}</code> .
Answer extraction	Brace-balanced search for the last occurrence of <code>\boxed{...}</code> ; if none is found, inspect the final ~300 characters of the output. Scan this region backwards and take the first occurrence of A–D (case-insensitive), then convert it to uppercase.
Grading	The predicted letter is compared with the gold key (case-insensitive). If no valid letter is found—or the output is blank—the item scores 0; otherwise it scores 1 when the letters match.

Table 19. Prompting and grading for DeepSeek 7B on MMLU.

Llama 8B + GSM8K

Aspect	Procedure
Prompt	Meta chat template. <i>System</i> : “You are a precise mathematician. Explain your reasoning step by step, then output ONLY the final number on a new line.” <i>User</i> : the GSM8K question.
Answer extraction	Inspect the model reply in order: (i) the last non-empty line of the response; (ii) if that fails, the final 25 whitespace-separated tokens. From the selected chunk, take the first integer-looking token (commas allowed, optional leading minus).
Grading	Numeric equality judged by the MIT-licensed PRM800K grader; every question is counted, and blank or unparsable answers score 0.

Table 20. Prompting and grading for Llama 8B on GSM8K.

Llama 8B + MMLU

Aspect	Procedure
Prompt	Meta chat template. <i>System</i> : “You are a knowledgeable and concise subject-matter expert. Work through the problem step by step. Finally, on a new line, output ONLY the single capital letter (A, B, C, or D) that corresponds to the correct choice.” <i>User</i> : the question followed by the four labeled choices A–D.
Answer extraction	Take the substring after the last newline and scan it left-to-right for the first capital A–D (case-insensitive). If none is found, inspect the final 10 whitespace-separated tokens of the whole response, scanning them right-to-left for A–D.
Grading	Predicted letter (upper-cased) is compared with the gold key. Every question is counted; if no valid letter is found or it does not match the gold answer, the item scores 0.

Table 21. Prompting and grading for Llama 8B on MMLU.

Llama 8B + RULER prompts

Aspect	Procedure
Prompt	Prompts are generated for the following RULER sub-tasks with a length of 4096–32768 tokens: fwe, niah_multivalued, qa_1, and qa_2. Greedy decoding is used. The model generates a maximum of 64 new tokens.
Grading	fwe: partial credit = (# of gold words present in the model output) / 3 (case-insensitive set match). niah_multivalued: take the first four unique integers from the model output; partial credit = (# of these that appear in the gold set) / 4. qa_1 and qa_2: correct if the gold answer string appears as a case-insensitive substring of the model output.

Table 22. Prompting and grading for Llama 8B on RULER prompts.

Licenses.

- **Models.** deepseek-ai/DeepSeek-R1-Distill-Qwen-7B (MIT) and meta-llama/Meta-Llama-3.1-8B-Instruct (Llama 3.1 license) on Hugging Face.
- **Datasets.** GSM8K openai/gsm8k (MIT) and MMLU cais/mmlu (MIT) on Hugging Face. RULER prompts (Apache).
- **Grader.** PRM800K numeric grader (MIT).

O. S^2 ANTA-prop pseudocode

Algorithm 2 provides a high-level overview of S^2 ANTA-prop. Algorithms 3, 4, and 5 show breakdowns of the kernels that perform score computation, sample budget allocation, and the V gather, respectively.

Algorithm 2 S^2 ANTA-prop (overview, decode/GQA): proportional tile budgets + systematic sparse- V

Require: $Q \in \mathbb{R}^{H \times d_k}$; $K, V \in \mathbb{R}^{n_k \times H_{kv} \times d_k}$ (GQA); tile length B_{tile} ; samples/head S .
Ensure: $O \in \mathbb{R}^{H \times d_k}$ approximating $\text{softmax}(QK^\top)V$.
 1: $T \leftarrow \lceil n_k/B_{\text{tile}} \rceil$, $G \leftarrow H/H_{kv}$, $k(h) \leftarrow \lfloor h/G \rfloor$, $\mathcal{T}_t = \lceil tB_{\text{tile}}, \min((t+1)B_{\text{tile}}, n_k) \rceil$.
 2: **Pass 1:** compute $m_{h,t} = \max_{n \in \mathcal{T}_t} s_{h,n}$ and $\ell_{h,t} = \sum_{n \in \mathcal{T}_t} \exp(s_{h,n} - m_{h,t})$; optionally stash $u_{h,n} = \exp(s_{h,n} - m_{h,t})$, where $s_{h,n} = Q_h^\top K_{n,k(h)}/\sqrt{d_k}$.
 3: **Budgets:** $m_h^* = \max_t m_{h,t}$; $W_{h,t} = \exp(m_{h,t} - m_h^*) \ell_{h,t}$; allocate integers $\{S_{h,t}\}_t$ with $\sum_t S_{h,t} = S$ and $S_{h,t} \approx S \cdot W_{h,t}/\sum_t W_{h,t}$ (largest remainder); set $\text{inv}\delta_{h,t} = S_{h,t}/\ell_{h,t}$ and $a_{0,h,t} \sim U[0,1)$.
 4: **Pass 2:** systematic counts $c_{h,n}$ from $x_{h,n} = \text{inv}\delta_{h,t} u_{h,n}$, then $O_h \leftarrow O_h + \sum_n c_{h,n} V_{n,k(h)}$.
 5: **return** O/S .

Algorithm 3 S^2 ANTA-prop, Kernel 1: pass-1 tile statistics (and optional u -stash)

Require: $Q \in \mathbb{R}^{H \times d_k}$; $K \in \mathbb{R}^{n_k \times H_{kv} \times d_k}$; tile length B_{tile} .
Ensure: $m \in \mathbb{R}^{H \times T}$, $\ell \in \mathbb{R}^{H \times T}$, and optional $u \in \mathbb{R}^{H \times n_k}$.
 1: $T \leftarrow \lceil n_k/B_{\text{tile}} \rceil$; $G \leftarrow H/H_{kv}$.
 2: **for** each KV head $k \in \{0, \dots, H_{kv}-1\}$ and tile $t \in \{0, \dots, T-1\}$ **in parallel do**
 3: $\mathcal{T}_t \leftarrow \lceil tB_{\text{tile}}, \min((t+1)B_{\text{tile}}, n_k) \rceil$.
 4: **for** each grouped head $g \in \{0, \dots, G-1\}$ **do**
 5: $h \leftarrow kG + g$; $s_{h,n} \leftarrow Q_h^\top K_{n,k}/\sqrt{d_k}$ for all $n \in \mathcal{T}_t$.
 6: $m_{h,t} \leftarrow \max_{n \in \mathcal{T}_t} s_{h,n}$; $\ell_{h,t} \leftarrow \sum_{n \in \mathcal{T}_t} \exp(s_{h,n} - m_{h,t})$.
 7: (Optional) $u_{h,n} \leftarrow \exp(s_{h,n} - m_{h,t})$ for all $n \in \mathcal{T}_t$.
 8: **end for**
 9: **end for**

Algorithm 4 S^2 ANTA-prop, Kernel 2: proportional per-tile budgets (largest remainder)

Require: Tile stats $m_{h,t}, \ell_{h,t}$; samples/head S ; seed.
Ensure: Integer budgets $S_{h,t}$ with $\sum_t S_{h,t} = S$, plus $\text{inv}\delta_{h,t}$ and offsets $a_{0,h,t}$.
 1: **for** each head $h \in \{0, \dots, H-1\}$ **in parallel do**
 2: $m_h^* \leftarrow \max_t m_{h,t}$.
 3: $W_{h,t} \leftarrow \exp(m_{h,t} - m_h^*) \ell_{h,t}$; $Z_h \leftarrow \sum_{t=0}^{T-1} W_{h,t}$.
 4: $q_t \leftarrow S \cdot W_{h,t}/Z_h$; $S_{h,t} \leftarrow \lfloor q_t \rfloor$ for all t .
 5: Give remaining $S - \sum_t S_{h,t}$ samples to tiles with largest fractional part of q_t (largest remainder).
 6: $\text{inv}\delta_{h,t} \leftarrow (S_{h,t} > 0) ? S_{h,t}/\ell_{h,t} : 0$; $a_{0,h,t} \sim \text{Unif}(0,1)$.
 7: **end for**

Algorithm 5 S^2 ANTA-prop, Kernel 3: systematic resampling and sparse- V accumulation (GQA grouped)

Require: $V \in \mathbb{R}^{n_k \times H_{kv} \times d_k}$; $u_{h,n}$; $\text{inv}\delta_{h,t}, a_{0,h,t}$; tile length B_{tile} .

Ensure: Accumulator $O \in \mathbb{R}^{H \times d_k}$ (fp32).

- 1: $G \leftarrow H/H_{kv}$; $O \leftarrow 0$.
- 2: **for** each KV head $k \in \{0, \dots, H_{kv}-1\}$ and tile $t \in \{0, \dots, T-1\}$ **in parallel do**
- 3: $\mathcal{T}_t \leftarrow \lceil tB_{\text{tile}}, \min((t+1)B_{\text{tile}}, n_k) \rceil$; heads $\mathcal{H}_k = \{kG, \dots, (k+1)G-1\}$.
- 4: **for** each head $h \in \mathcal{H}_k$ **do**
- 5: $p \leftarrow 0$.
- 6: **for** each $n \in \mathcal{T}_t$ (increasing) **do**
- 7: $x \leftarrow \text{inv}\delta_{h,t} u_{h,n}$.
- 8: $c_{h,n} \leftarrow \lfloor a_{0,h,t} + p + x \rfloor - \lfloor a_{0,h,t} + p \rfloor$; $p \leftarrow p + x$.
- 9: **end for**
- 10: **end for**
- 11: (Optional) compact emitted rows $\mathcal{E}_t = \{n \in \mathcal{T}_t : \exists h \in \mathcal{H}_k, c_{h,n} > 0\}$.
- 12: **for** each $n \in \mathcal{E}_t$ and each $h \in \mathcal{H}_k$ **do**
- 13: $O_h \leftarrow O_h + c_{h,n} V_{n,k}$.
- 14: **end for**
- 15: **end for**
- 16: **return** O (apply final scaling by $1/S$ outside or in a final cast/scale kernel).

P. S^2 ANTA-flash pseudocode

Algorithm 6 provides a high-level overview of S^2 ANTA-flash. Algorithms 7 and 8 describe the 2 kernels that constitute S^2 ANTA-flash in detail.

Algorithm 6 S^2 ANTA-flash (overview, decode/GQA): uniform per-tile sampling + FlashDecoding-style merge

Require: $Q \in \mathbb{R}^{H \times d_k}$; $K, V \in \mathbb{R}^{n_k \times H_{kv} \times d_k}$ (GQA); tile length B_{tile} ; samples/head S ; seed.

Ensure: $O \in \mathbb{R}^{H \times d_k}$ approximating $\text{softmax}(QK^T)V$.

- 1: $T \leftarrow \lceil n_k/B_{\text{tile}} \rceil$; $G \leftarrow H/H_{kv}$; $k(h) \leftarrow \lfloor h/G \rfloor$; uniform per-tile budget $S_{\text{tile}} \approx S/T$ (rounded).
- 2: **Kernel 1 (tile partials):** for each tile (k, t) , compute $(m_{h,t}, \ell_{h,t})$ and $\tilde{O}_{h,t} = \sum_{n \in \mathcal{T}_t} c_{h,n} V_{n,k}$ via systematic sampling with budget S_{tile} .
- 3: **Kernel 2 (merge):** for each head h , set $m_h^* = \max_t m_{h,t}$, $W_{h,t} = \exp(m_{h,t} - m_h^*) \ell_{h,t}$, $Z_h = \sum_t W_{h,t}$, and $O_h = \frac{1}{Z_h} \sum_t W_{h,t} (\tilde{O}_{h,t}/S_{\text{tile}})$.
- 4: **return** O .

Algorithm 7 S^2 ANTA-flash, Kernel 1: fused per-tile partials (stats + systematic sampling)

Require: $Q \in \mathbb{R}^{H \times d_k}$; $K, V \in \mathbb{R}^{n_k \times H_{kv} \times d_k}$; tile length B_{tile} ; samples/head S ; seed.

Ensure: Per-tile outputs $(m_{h,t}, \ell_{h,t}, \tilde{O}_{h,t})$ for all heads and tiles.

- 1: $T \leftarrow \lceil n_k/B_{\text{tile}} \rceil$; $G \leftarrow H/H_{kv}$; $S_{\text{tile}} \approx S/T$ (rounded).
- 2: **for** each KV head $k \in \{0, \dots, H_{kv}-1\}$ and tile $t \in \{0, \dots, T-1\}$ **in parallel do**
- 3: $\mathcal{T}_t \leftarrow \lceil tB_{\text{tile}}, \min((t+1)B_{\text{tile}}, n_k) \rceil$; heads $\mathcal{H}_k = \{kG, \dots, (k+1)G-1\}$.
- 4: **for** each head $h \in \mathcal{H}_k$ **do**
- 5: $s_{h,n} \leftarrow Q_h^\top K_{n,k} / \sqrt{d_k}$ for $n \in \mathcal{T}_t$.
- 6: $m_{h,t} \leftarrow \max_{n \in \mathcal{T}_t} s_{h,n}$; $u_{h,n} \leftarrow \exp(s_{h,n} - m_{h,t})$;
- 7: $\ell_{h,t} \leftarrow \sum_{n \in \mathcal{T}_t} u_{h,n}$.
- 8: $\text{inv}\delta_{h,t} \leftarrow (S_{\text{tile}}/\ell_{h,t})$ (or 0 if $\ell_{h,t}$ is tiny); $a_{0,h,t} \sim U[0, 1)$.
- 9: Use systematic counts $c_{h,n}$ from $x_{h,n} = \text{inv}\delta_{h,t} u_{h,n}$ and accumulate $\tilde{O}_{h,t} \leftarrow \sum_{n \in \mathcal{T}_t} c_{h,n} V_{n,k}$.
- 10: **end for**

Algorithm 8 S^2 ANTA-flash, Kernel 2: FlashAttention-style merge across tiles

Require: Per-tile $(m_{h,t}, \ell_{h,t}, \tilde{O}_{h,t})$ from Alg. 7; S_{tile} .

Ensure: Final $O \in \mathbb{R}^{H \times d_k}$.

- 1: **for** each head $h \in \{0, \dots, H-1\}$ **in parallel do**
- 2: $m_h^* \leftarrow \max_t m_{h,t}$.
- 3: $W_{h,t} \leftarrow \exp(m_{h,t} - m_h^*) \ell_{h,t}$; $Z_h \leftarrow \sum_{t=0}^{T-1} W_{h,t}$.
- 4: $O_h \leftarrow \frac{1}{Z_h} \sum_{t=0}^{T-1} W_{h,t} (\tilde{O}_{h,t}/S_{\text{tile}})$.
- 5: **end for**
- 6: **return** O .

Q. Decode-step kernel microbenchmark details

This appendix describes the microbenchmark used to measure *decode-step* attention latency for FlashAttention2 decoding (“FlashDecoding”), FlashInfer decoding, and our custom S^2 ANTA CUDA kernels. The intent is to be explicit about tensor shapes, software/hardware environment, cache state, and what is (and is not) included in the reported runtimes, in order to support a fair comparison.

What is being measured. We measure GPU kernel time for a single decoding step (one new token) as a function of the KV-cache length n_k . Timing is performed with CUDA events, recorded on the active CUDA stream and synchronized on the end event each iteration. The reported milliseconds therefore reflect elapsed time on the GPU timeline for the CUDA work launched by a single backend call (which may internally launch multiple kernels). All Python/CPU overhead and input construction are excluded by allocating and populating tensors outside the timed region and recording events immediately around the backend call.

Hardware and driver. All measurements were run on a single **NVIDIA RTX 6000 Ada Generation** GPU (48 GB). The installed driver reported by `nvidia-smi` was 580.82.07 (CUDA compatibility reported as 13.0).

Software environment (versions). The benchmark environment used:

- **PyTorch 2.6.0+cu124**
- **flash-attn 2.7.3** (FlashAttention2)
- **flashinfer-python 0.5.3**

Our S^2 ANTA kernels are invoked through a PyTorch CUDA extension (custom CUDA code callable from PyTorch); the timed region includes all CUDA kernels launched by this extension entrypoint.

Decode geometry and tensor shapes. We benchmark a single-batch decode step with head geometry matching a Llama-style GQA configuration:

$$H = 32, \quad H_{kv} = 8, \quad d_k = 128, \quad G = H/H_{kv} = 4,$$

where H is the number of query heads, H_{kv} is the number of KV heads, and d_k is the head dimension. The query length is one token (decode), batch size is one, and attention is causal.

For each cache length n_k , the following tensors are constructed once and reused across timing iterations:

- Query tensor with shape $[H, d_k]$.
- Key/value cache tensors stored in a sequence-major layout with shape $[n_k+1, H_{kv}, d_k]$. (The extra $+1$ slot corresponds to the current token.)

All backends are run with the same causal setting and the standard softmax scaling $1/\sqrt{d_k}$, with dropout disabled.

Input distribution and dtype. All inputs are i.i.d. Gaussian (`torch.randn`) generated directly on the GPU. Unless otherwise stated, the query, keys, and values are provided in bfloat16 (the harness also supports fp16). A fixed RNG seed is used so that, for a given n_k , each backend sees the same input tensors.

Cold-cache protocol (L2 thrashing). To reduce sensitivity to favorable cache residency effects: before *each* timed iteration, we touch a large GPU buffer by performing an in-place update on a 512 MB float32 tensor. This operation is intended to thrash GPU caches (including L2) via a large read+write stream. The cache-thrash operation is executed *outside* the timed region (before the start event is recorded), and therefore is not included in the reported kernel time.

Timing protocol and trial structure. For each cache length n_k and each backend, we run a fixed number of warmup and timed iterations:

- **Warmup:** 10 untimed iterations to amortize one-time effects (e.g., kernel selection/caching inside libraries).
- **Timing:** 40 timed iterations. Each iteration performs an optional cache-thrash (not timed), then records a start CUDA event, launches the backend once, records an end CUDA event, synchronizes on the end event, and reads elapsed milliseconds from the event pair.
- **Aggregation:** we report the mean latency over the 40 timed iterations.

All tensor allocations and concatenations/appends used to construct inputs are performed outside the timed region.

Note on KV-cache appends in FlashDecoding. FlashAttention2 decoding performs a fused KV-cache append/update as part of its decode call, whereas FlashInfer decoding and our S^2 ANTA decode kernels do not perform an internal append in this benchmark. To isolate the attention-like decode computation for FlashInfer and S^2 ANTA, we provide a cache tensor that already includes the current token in the preallocated $[n_k+1, H_{kv}, d_k]$ storage.

This asymmetry is not material in the long-context regime: the fused append cost is $O(H_{kv}d_k)$ per step and does not scale with n_k , so its fractional contribution decreases as n_k grows. Our speedup comparisons focus on large KV-cache lengths (e.g., 8k–32k tokens), where the attention computation dominates. Including the fused append inside FlashDecoding therefore does not change qualitative conclusions in this regime (and makes the FlashDecoding measurement slightly more conservative relative to an “attention-only” timing).

R. Additional S^2 ANTA kernel results

Table 23. Accuracy of Llama 8B on 4 long-context tasks with an 8k-token prompt. Tasks: frequent word extraction (FWE), needle-in-a-haystack (NIAH), single-hop QA (QA₁), multi-hop QA (QA₂). S : sample budget. Accuracy shows 95% bootstrap confidence intervals.

Kernel	S	FWE	NIAH	QA ₁	QA ₂
S^2 ANTA-prop	64	96.60±0.52	93.23±0.69	70.73±2.43	67.33±2.46
S^2ANTA-prop	128	98.04±0.40	93.78±0.60	70.33±2.40	66.87±2.43
S^2 ANTA-prop	256	98.07±0.40	94.05±0.62	70.67±2.33	66.40±2.30
S^2 ANTA-flash	64	66.47±1.12	83.57±1.05	65.67±2.44	62.27±2.40
S^2 ANTA-flash	128	86.11±0.91	91.70±0.73	69.47±2.30	66.27±2.50
S^2 ANTA-flash	256	94.80±0.62	92.77±0.63	70.67±2.20	66.80±2.50
S^2ANTA-flash	1024	98.11±0.40	94.22±0.58	70.73±2.30	66.33±2.40
SDPA (baseline)	—	98.53±0.60	94.55±1.00	71.80±3.90	68.60±4.20

References

- Ainslie, J., Lee-Thorp, J., de Jong, M., Zemlyanskiy, Y., Lebron, F., and Sanghai, S. Gqa: Training generalized multi-query transformer models from multi-head checkpoints. In *The 2023 Conference on Empirical Methods in Natural Language Processing*, 2023.
- Beltagy, I., Peters, M. E., and Cohan, A. Longformer: The long-document transformer. *arXiv preprint arXiv:2004.05150*, 2020.
- Boucheron, S., Lugosi, G., and Massart, P. *Concentration Inequalities: A Nonasymptotic Theory of Independence*. Oxford University Press, Oxford, 2013.
- Center for AI Safety. MMLU: Massive multitask language understanding dataset. <https://huggingface.co/datasets/cais/mmlu>, 2024. MIT license. Commit c30699e (uploaded 2024-03-08). Accessed 2025-05-14.
- Chen, Z., Sadhukhan, R., Ye, Z., Zhou, Y., Zhang, J., Nolte, N., Tian, Y., Douze, M., Bottou, L., Jia, Z., and Chen, B. MagicPIG: LSH sampling for efficient LLM generation. In *The Thirteenth International Conference on Learning Representations*, 2025. URL <https://openreview.net/forum?id=ALzTQUgW8a>.
- Child, R., Gray, S., Radford, A., and Sutskever, I. Generating long sequences with sparse transformers. *arXiv preprint arXiv:1904.10509*, 2019.
- Clark, K., Khandelwal, U., Levy, O., and Manning, C. D. What does BERT look at? an analysis of BERT’s attention. In Linzen, T., Chrupala, G., Belinkov, Y., and Hupkes, D. (eds.), *Proceedings of the 2019 ACL Workshop BlackboxNLP: Analyzing and Interpreting Neural Networks for NLP*, pp. 276–286, Florence, Italy, August 2019. Association for Computational Linguistics. doi: 10.18653/v1/W19-4828. URL <https://aclanthology.org/W19-4828/>.
- Cobbe, K., Kosaraju, V., Bavarian, M., Chen, M., Jun, H., Kaiser, L., Plappert, M., Tworek, J., Hilton, J., Nakano, R., et al. Training verifiers to solve math word problems. *arXiv preprint arXiv:2110.14168*, 2021.
- Cochran, W. G. *Sampling Techniques*. Wiley, New York, 3rd edition, 1977.
- Dao, T., Haziza, D., Massa, F., and Sizov, G. Flash-Decoding for long-context inference. <https://crfm.stanford.edu/2023/10/12/flashdecoding.html>, October 2023. Stanford Center for Research on Foundation Models (CRFM) blog post, accessed 2026-01-20.
- DeepSeek-AI. Deepseek-r1: Incentivizing reasoning capability in llms via reinforcement learning, 2025. URL <https://arxiv.org/abs/2501.12948>.
- Dettmers, T., Pagnoni, A., Holtzman, A., and Zettlemoyer, L. Qlora: Efficient finetuning of quantized llms. *Advances in neural information processing systems*, 36:10088–10115, 2023.
- Frantar, E., Ashkboos, S., Hoefler, T., and Alistarh, D. OPTQ: Accurate quantization for generative pre-trained transformers. In *The Eleventh International Conference on Learning Representations*, 2023. URL <https://openreview.net/forum?id=tcbBPnfwxS>.
- Gemini Team, Anil, R., Borgeaud, S., Alayrac, J.-B., Yu, J., Soricut, R., Schalkwyk, J., Dai, A. M., Hauth, A., Millican, K., et al. Gemini: a family of highly capable multimodal models. *arXiv preprint arXiv:2312.11805*, 2023.
- Gupta, A., Dar, G., Goodman, S., Ciprut, D., and Berant, J. Memory-efficient transformers via top-k attention. In Moosavi, N. S., Gurevych, I., Fan, A., Wolf, T., Hou, Y., Marasović, A., and Ravi, S. (eds.), *Proceedings of the Second Workshop on Simple and Efficient Natural Language Processing*, pp. 39–52, Virtual, November 2021. Association for Computational Linguistics. doi: 10.18653/v1/2021.sustainlp-1.5. URL <https://aclanthology.org/2021.sustainlp-1.5/>.
- Hendrycks, D., Burns, C., Basart, S., Zou, A., Mazeika, M., Song, D., and Steinhardt, J. Measuring massive multitask language understanding. In *International Conference on Learning Representations*, 2021. URL <https://openreview.net/forum?id=d7KBjmI3GmQ>.
- Hooper, C., Kim, S., Mohammadzadeh, H., Mahoney, M. W., Shao, Y. S., Keutzer, K., and Gholami, A. Kvquant: Towards 10 million context length llm inference with kv cache quantization. *Advances in Neural Information Processing Systems*, 37:1270–1303, 2024.
- Horowitz, M. 1.1 computing’s energy problem (and what we can do about it). In *2014 IEEE International Solid-State Circuits Conference Digest of Technical Papers (ISSCC)*, pp. 10–14, 2014. doi: 10.1109/ISSCC.2014.6757323.
- Hsieh, C.-P., Sun, S., Krizan, S., Acharya, S., Rekish, D., Jia, F., and Ginsburg, B. Ruler: What’s the real context size of your long-context language models? In *First Conference on Language Modeling*, 2024.
- Kim, H. and Ko, J. Fast monte-carlo approximation of the attention mechanism. In *Proceedings of the AAAI conference on artificial intelligence*, volume 36, pp. 7185–7193, 2022.

- Kitaev, N., Kaiser, L., and Levskaya, A. Reformer: The efficient transformer. In *International Conference on Learning Representations*, 2020. URL <https://openreview.net/forum?id=rkgNKkHtvB>.
- Lightman, H., Kosaraju, V., Burda, Y., Edwards, H., Baker, B., Lee, T., Leike, J., Schulman, J., Sutskever, I., and Cobbe, K. Let’s verify step by step. In *The Twelfth International Conference on Learning Representations*, 2024. URL <https://openreview.net/forum?id=v8L0pN6EOi>.
- Liu, Z., Yuan, J., Jin, H., Zhong, S., Xu, Z., Braverman, V., Chen, B., and Hu, X. Kivi: A tuning-free asymmetric 2bit quantization for kv cache. In *International Conference on Machine Learning*, pp. 32332–32344. PMLR, 2024.
- Lohr, S. L. *Sampling: Design and Analysis*. Brooks/Cole, Boston, 2nd edition, 2010.
- Ma, S., Wang, H., Huang, S., Zhang, X., Hu, Y., Song, T., Xia, Y., and Wei, F. Bitnet b1.58 2b4t technical report, 2025. URL <https://arxiv.org/abs/2504.12285>.
- Meta AI. Meta Llama 3.1 8B Instruct: Version 1. <https://huggingface.co/meta-llama/Llama-3.1-8B-Instruct>, 2024. Llama 3.1 Community License. Model release 2024-07-23. Accessed 2025-05-14.
- OpenAI. Gpt-4 technical report, 2023. URL <https://arxiv.org/abs/2303.08774>.
- OpenAI. GSM8K: Grade school math word problems (v1.0). <https://huggingface.co/datasets/openai/gsm8k>, 2023. MIT License, commit e53f048. Accessed 2025-05-14.
- Owen, A. B. *Monte Carlo Theory, Methods and Examples*. 2013. Monograph.
- Pinelis, I. Optimum bounds for the distributions of martingales in banach spaces. *The Annals of Probability*, 22(4): 1679–1706, 1994.
- Rajpurkar, P., Jia, R., and Liang, P. Know what you don’t know: Unanswerable questions for SQuAD. In Gurevych, I. and Miyao, Y. (eds.), *Proceedings of the 56th Annual Meeting of the Association for Computational Linguistics (Volume 2: Short Papers)*, pp. 784–789, Melbourne, Australia, July 2018. Association for Computational Linguistics. doi: 10.18653/v1/P18-2124. URL <https://aclanthology.org/P18-2124/>.
- Ribar, L., Chelombiev, I., Hudlass-Galley, L., Blake, C., Luschi, C., and Orr, D. Sparq attention: Bandwidth-efficient llm inference. In *International Conference on Machine Learning*, pp. 42558–42583. PMLR, 2024.
- Samaga B L, Y., Yerram, V., You, C., Bhojanapalli, S., Kumar, S., Jain, P., and Netrapalli, P. Hire: High recall approximate top- k estimation for efficient llm inference, 2024. URL <https://arxiv.org/abs/2402.09360>.
- Sun, H., Chen, Z., Yang, X., Tian, Y., and Chen, B. Triforce: Lossless acceleration of long sequence generation with hierarchical speculative decoding. In *First Conference on Language Modeling*, 2024.
- Tang, J., Zhao, Y., Zhu, K., Xiao, G., Kasikci, B., and Han, S. Quest: query-aware sparsity for efficient long-context llm inference. In *Proceedings of the 41st International Conference on Machine Learning*, pp. 47901–47911, 2024.
- Touvron, H., Lavril, T., Izacard, G., Martinet, X., Lachaux, M.-A., Lacroix, T., Rozière, B., Goyal, N., Hambro, E., Azhar, F., Rodriguez, A., Joulin, A., Grave, E., and Lample, G. Llama: Open and efficient foundation language models, 2023. URL <https://arxiv.org/abs/2302.13971>.
- Vaswani, A., Shazeer, N., Parmar, N., Uszkoreit, J., Jones, L., Gomez, A. N., Kaiser, Ł., and Polosukhin, I. Attention is all you need. *Advances in neural information processing systems*, 30, 2017.
- Wang, S., Li, B. Z., Khabsa, M., Fang, H., and Ma, H. Linformer: Self-attention with linear complexity. *arXiv preprint arXiv:2006.04768*, 2020.
- Williams, R. J. Simple statistical gradient-following algorithms for connectionist reinforcement learning. *Machine Learning*, 8(3-4):229–256, 1992.
- Xie, X., Luo, Y., Peng, H., and Ding, C. RTop-k: Ultra-fast row-wise top-k selection for neural network acceleration on GPUs. In *The Thirteenth International Conference on Learning Representations*, 2025. URL <https://openreview.net/forum?id=PHg4rAXFVH>.
- Yang, Z., Qi, P., Zhang, S., Bengio, Y., Cohen, W., Salakhutdinov, R., and Manning, C. D. HotpotQA: A dataset for diverse, explainable multi-hop question answering. In Riloff, E., Chiang, D., Hockenmaier, J., and Tsujii, J. (eds.), *Proceedings of the 2018 Conference on Empirical Methods in Natural Language Processing*, pp. 2369–2380, Brussels, Belgium, October–November 2018. Association for Computational Linguistics. doi: 10.18653/v1/D18-1259. URL <https://aclanthology.org/D18-1259/>.
- Ye, Z., Chen, L., Lai, R., Lin, W., Zhang, Y., Wang, S., Chen, T., Kasikci, B., Grover, V., Krishnamurthy, A., and Ceze, L. Flashinfer: Efficient and customizable attention engine for LLM inference serving. In *Eighth Conference*

on *Machine Learning and Systems*, 2025. URL <https://openreview.net/forum?id=RXPopAsL8F>.

Zaheer, M., Guruganesh, G., Dubey, K. A., Ainslie, J., Alberti, C., Ontanon, S., Pham, P., Ravula, A., Wang, Q., Yang, L., et al. Big bird: Transformers for longer sequences. *Advances in neural information processing systems*, 33:17283–17297, 2020.

Zhang, Z., Sheng, Y., Zhou, T., Chen, T., Zheng, L., Cai, R., Song, Z., Tian, Y., Ré, C., Barrett, C., et al. H2o: Heavy-hitter oracle for efficient generative inference of large language models. *Advances in Neural Information Processing Systems*, 36:34661–34710, 2023.